Mössbauer mineralogy of rock, soil, and dust at Gusev crater, Mars: Spirit's journey through weakly altered olivine basalt on the plains and pervasively altered basalt in the Columbia Hills

R. V. Morris,[1] G. Klingelhöfer,[2] C. Schröder,[2] D. S. Rodionov,[2,3] A. Yen,[4] D. W. Ming,[1] P. A. de Souza Jr.,[2,5] I. Fleischer,[2] T. Wdowiak,[6] R. Gellert,[7] B. Bernhardt,[2] E. N. Evlanov,[3] B. Zubkov,[3] J. Foh,[2,8] U. Bonnes,[8] E. Kankeleit,[8] P. Gütlich,[2] F. Renz,[2] S. W. Squyres,[9] and R. E. Arvidson[10]

Received 1 September 2005; revised 21 October 2005; accepted 9 December 2005; published 22 February 2006.

[1] The Mössbauer spectrometer on Spirit measured the oxidation state of Fe, identified Fe-bearing phases, and measured relative abundances of Fe among those phases for surface materials on the plains and in the Columbia Hills of Gusev crater. Eight Fe-bearing phases were identified: olivine, pyroxene, ilmenite, magnetite, nanophase ferric oxide (npOx), hematite, goethite, and a Fe^{3+}-sulfate. Adirondack basaltic rocks on the plains are nearly unaltered ($Fe^{3+}/Fe_T < 0.2$) with Fe from olivine, pyroxene (Ol > Px), and minor npOx and magnetite. Columbia Hills basaltic rocks are nearly unaltered (Peace and Backstay), moderately altered (WoolyPatch, Wishstone, and Keystone), and pervasively altered (e.g., Clovis, Uchben, Watchtower, Keel, and Paros with $Fe^{3+}/Fe_T \sim 0.6–0.9$). Fe from pyroxene is greater than Fe from olivine (Ol sometimes absent), and Fe^{2+} from Ol + Px is 40–49% and 9–24% for moderately and pervasively altered materials, respectively. Ilmenite (Fe from Ilm ~3–6%) is present in Backstay, Wishstone, Keystone, and related rocks along with magnetite (Fe from Mt ~10–15%). Remaining Fe is present as npOx, hematite, and goethite in variable proportions. Clovis has the highest goethite content (Fe from Gt = 40%). Goethite (α-FeOOH) is mineralogical evidence for aqueous processes because it has structural hydroxide and is formed under aqueous conditions. Relatively unaltered basaltic soils ($Fe^{3+}/Fe_T \sim 0.3$) occur throughout Gusev crater (~60–80% Fe from Ol + Px, ~10–30% from npOx, and ~10% from Mt). PasoRobles soil in the Columbia Hills has a unique occurrence of high concentrations of Fe^{3+}-sulfate (~65% of Fe). Magnetite is identified as a strongly magnetic phase in Martian soil and dust.

Citation: Morris, R. V., et al. (2006), Mössbauer mineralogy of rock, soil, and dust at Gusev crater, Mars: Spirit's journey through weakly altered olivine basalt on the plains and pervasively altered basalt in the Columbia Hills, *J. Geophys. Res.*, *111*, E02S13, doi:10.1029/2005JE002584.

1. Introduction

[2] The Mars Exploration Rover (MER) Spirit landed on the plains of the Noachian-age, 160-km-diameter Gusev crater at 14.5692°S, 175.4729°E in International Astronomical Union 2000 coordinates on 4 January 2004 UTC [*Squyres et al.*, 2004; *Arvidson et al.*, 2004]. The primary scientific objective of Spirit's exploration is to characterize the surface and atmosphere, searching for evidence of water and clues for assessing past and current climates and their suitability for life [*Squyres et al.*, 2004]. The Athena science payload on Spirit carries as mast-mounted remote-sensing instruments a panoramic, multispectral camera (Pancam) and a miniature thermal emission spectrometer (Mini-TES) and, as in situ instruments mounted on a 5-degree-of-freedom robotic arm, an Alpha Particle X-Ray Spectrometer (APXS), a Microscopic Imager (MI), a Rock Abrasion Tool (RAT), and, the focus of this paper, a miniature

[1]NASA Johnson Space Center, Houston, Texas, USA.
[2]Institut für Anorganische und Analytische Chemie, Johannes Gutenberg-Universität, Mainz, Germany.
[3]Space Research Institute IKI, Moscow, Russia.
[4]Jet Propulsion Laboratory, California Institute of Technology, Pasadena, California, USA.
[5]CVRD Group, Vitoria, Brazil.
[6]Department of Physics, University of Alabama at Birmingham, Birmingham, Alabama, USA.
[7]Department of Physics, University of Guelph, Guelph, Ontario, Canada.
[8]Darmstadt University of Technology, Darmstadt, Germany.
[9]Center for Radiophysics and Space Research, Cornell University, Ithaca, New York, USA.
[10]Department of Earth and Planetary Sciences, Washington University, St. Louis, Missouri, USA.

0148-0227/06/2005JE002584$09.00

Mössbauer spectrometer (MIMOS II) [*Squyres et al.*, 2003; *Klingelhöfer et al.*, 2003].

[3] Mössbauer (MB) spectrometers provide quantitative information about the distribution of Fe among its oxidation and coordination states (e.g., octahedrally coordinated Fe^{3+}), identification of Fe-bearing phases, and relative distribution of Fe among those phases. Ferrous iron (Fe^{2+}) is present in both primary silicate and oxide minerals (e.g., olivine, pyroxene, ilmenite, and (titano)magnetite) and secondary minerals (e.g., serpentine and sulfates). Although present at significant levels in some primary phases (e.g., augite and (titano)magnetite), ferric iron (Fe^{3+}) is commonly a product of oxidative alteration and weathering of primary minerals and often occurs as oxides and oxyhydroxides. The speciation and distribution of Fe in Martian rock and soil thus constrain the primary rock type (e.g., olivine- versus pyroxene-bearing basalt), the redox conditions under which primary minerals crystallized (e.g., presence or absence of magnetite), the extent of alteration and weathering (e.g., value of Fe^{3+}/Fe_T), the type of alteration and weathering products (e.g., oxides versus sulfates versus phyllosilicates), and the processes and environmental conditions for alteration and weathering (e.g., neutral versus acid-chloride versus acid-sulfate aqueous process under ambient or hydrothermal conditions [e.g., *Morris et al.*, 2000]).

[4] Preliminary results from Spirit's Mössbauer instrument are reported by *Morris et al.* [2004] as part of a special journal issue on the results of the primary mission (first 90 sols). In the current paper, we report results for the first 510 sols of Spirit's exploration, which includes a relatively flat journey across the Gusev plains to West Spur on the flank of the Columbia Hills (sol 156), and then a climb up to near the summit of Husband Hill via West Spur and Cumberland ridge. *Arvidson et al.* [2006] provide a summary of mission operations and payload measurement campaigns for Spirit through sol 512 and a synopsis of key scientific findings derived from all elements of the Athena Payload.

2. Instrument, Measurement, and Spectral Analysis

2.1. Instrument and Measurement

[5] Instrumental considerations for the MER MIMOS II Mössbauer spectrometers are described in detail by *Klingelhöfer et al.* [2003]. Briefly, Spirit's spectrometer has 512 data channels, operates in backscatter geometry with a triangular waveform at a drive frequency of ~24 Hz and a standard (but selectable) calibrated velocity range of ±12 mm/s, and has a primary ^{57}Co gamma radiation source with an intensity of ~300 mCi at launch (~30 mCi on sol 510). Velocity calibration was performed on the surface of Mars using spectra of an absorber (internal to the instrument) of metallic Fe foil, hematite, and magnetite that were acquired in transmission geometry simultaneously with measurements on surface targets. Simultaneous measurements are possible because the primary (target) and secondary (calibration) ^{57}Co sources are mounted at opposite ends of the velocity transducer. The maximum velocity values V_{max} for different drive voltage settings were determined from the center positions of the metallic Fe-foil and hematite lines which were obtained by fitting the spectra of the internal reference absorber. This results in a linear velocity scale which is corrected for the nonlinear behavior of the drive system by using the measured drive error signal. This error signal (i.e., the deviation from actual velocity from the ideal waveform velocity), measured in mV/channel, is directly proportional to the deviation (in mm/s) from the linear velocity scale, and therefore was used to obtain the actual, nonlinear velocity scale.

[6] The spectrometer is placed into physical contact with surface targets by the robotic arm, with contact being sensed by the closing of two individual micro switches on a spring-loaded contact plate. Assuming a flat surface below the contact plate, the target area illuminated by the incident 14.4 keV ^{57}Co gamma radiation has a diameter of ~1.5 cm. The sampling depth in basaltic materials is ~0.03 g/cm^2, or ~3 mm in air-fall dust and ~0.2 mm for coherent rock [*Klingelhöfer et al.*, 2003]. Temperature sensors are located on the contact plate and a location proximate to the metallic Fe foil sample to measure the temperature of the surface target and the metallic Fe foil standard, respectively. The two temperature sensors normally record the same temperature to within 10 K. A third temperature sensor is located on the MB electronics board in Spirit's warm electronics box. Because of diurnal temperature variations on Mars, MIMOS II stores spectral data in 13 separate memory areas that correspond to 11 temperature windows 10 K wide between 180 and 290 K plus windows for data acquired above and below these temperatures. The 6.4 keV resonantly scattered X-rays and the 14.4 keV resonantly scattered γ-rays from surface targets are detected by the four instrument detectors. Because there are only four counters available (a fifth stores spectra from the reference absorber), the spectral data are summed in a way that is configurable by command from the Earth. Through sol 461, the detector counters were configured to sum, pairwise, 6.4 and 14.4 keV data. This configuration returned both 6.4 and 14.4 keV data to the Earth. After sol 461, each counter was commanded to store data from only 14.4 keV energy windows (one counter per detector), returning only 14.4 keV data to Earth. This configuration permits maximum spatial resolution to look for orientation effects using the higher signal-to-noise ratio of the 14.4 keV detectors. The number of baseline counts in the 6.4 keV energy window is typically three times that in the 14.4 keV window, resulting in a lower signal-to-noise ratio for the former. Only 14.4 keV MB spectra are discussed in this paper.

[7] At the start of the mission when the ^{57}Co source was strong, it was possible to do quick touch-and-go reconnaissance Mössbauer integrations for 1–2 hr at the beginning of a sol in addition to the normal overnight integrations. At this time in the mission (beyond sol 510), touch-and-go integrations are not sensible because of very poor counting statistics, and 48 hr integrations are the norm. Whenever possible, coupled observations of the same target are made by all MER analytical instruments, in order to maximize synergism.

2.2. Spectral Analysis

[8] The Mössbauer parameters for component subspectra that are relevant for oxidation state, coordination state, and phase identification are the isomer shift (δ) and quadrupole splitting (ΔE_Q) for doublets and δ, ΔE_Q, and the magnetic

hyperfine field strength (B_{hf}) for sextets. Peak line widths (FWHM, full width at half-maximum intensity) can provide information on whether a subspectrum is from a single, well-defined site or a distribution of closely related sites. Subspectral areas (A) provide information about the distribution of Fe among oxidation and coordination states and among iron-bearing phases in the target. Subspectral areas do not provide information about the proportion of the iron-bearing phases themselves, unless the concentration of Fe in those phases is independently known or modeled. For doublet spectra, $\delta = 1/2(v_1 + v_2)$ and $\Delta E_Q = |v_2 - v_1|$, where v_1 and v_2 are center positions of the doublet peaks numbered from minimum to maximum velocity. For sextet spectra, $\delta = 1/4(v_1 + v_2 + v_5 + v_6)$, $\Delta E_Q = 1/2((v_6 - v_5) - (v_2 - v_1))$, and B_{hf} = constant x ($|v_6 - v_1|$), where $v_1, \ldots, v_6$ are the center positions of the sextet peaks numbered from minimum to maximum velocity. Assuming good counting statistics, the center positions were calculated using a variety of commercial and in-house least squares fitting computer programs where, for example, the peak line shape function, center, width, and area are adjustable parameters. In laboratory environments, the counting statistics can be made arbitrarily good by long counting times and/or by using strong ^{57}Co sources. On Mars, arbitrarily long counting times are not possible within timely progression of mission science requirements, and a weak ^{57}Co source cannot be replaced by a strong one.

[9] Our choices for improving counting statistics in MER spectra are either to sum the data for all or a subset of temperature windows for measurements of a single target or to sum data for the same temperature interval (one or more temperature windows) from measurements of multiple targets. If the Mössbauer parameters are strongly dependent on temperature, summing over a wide temperature interval will broaden peaks, leading to reduced velocity resolution. Summing spectra over multiple targets for individual temperature windows will not broaden peaks if the mineralogical composition is invariant, and the subspectral areas will be the weighted average for the aggregate. Subspectral areas of the individual targets would then be calculated using the information previously obtained (e.g., δ, ΔE_Q, and B_{hf}) as fitting constraints. We employed both approaches.

[10] As will be discussed in the next section, 5 doublet and 4 sextet subspectra were required to fit MB spectra from 86 targets. This corresponds to ~2064 individual MB spectra because the instrument has 4 counters for acquiring spectra and each target analysis typically has spectra for 6 temperature windows. Not all 9 subspectra are present in every spectrum. The complexity of the spectra ranges from 3 doublet subspectra (6 peaks) to 3 doublet and 4 sextet subspectra (30 peaks). Even with the above measures to improve counting statistics, they were still marginal for low-intensity peaks, which commonly occurred for sextet subspectra. Fortunately, there were targets where each subspectrum contributed significant subspectral area so that its MB parameters could be calculated and used as fitting constraints in spectra where the subspectrum is a minor component.

[11] The constraints used during fitting procedures are discussed next. We here use generic names for the subspectra and discuss their assignment in terms of Fe oxidation state, coordination state, and phase assignment in the next section. The generic subspectral names have the format FeXYZ, where X = 2, 2.5, or 3 depending on the oxidation state of Fe, Y = D or S (doublet or sextet), and Z is a sequential number for subspectra having the same FeXY. All spectra were independently fit by at least two authors of this paper using two approaches to determine peak centers during the computations. In one approach, the peak centers were fit and the MB parameters (δ, ΔE_Q, and B_{hf}) calculated from the fit peak positions; in the other approach, the MB parameters were fit and peak positions calculated from the MB parameters. Distribution functions can be used when MB parameters are fit. The values of the MB parameters that we report are averages of the values obtained in these independent fits, and the parameter errors are the larger of the statistical error (not often) or the deviation from average value of the independent fits. Minimum errors we report are ±0.02 mm/s for δ and ΔE_Q, ±0.8 T for B_{hf} and ±2% (absolute) for A.

[12] There are a number of fitting constraints that we always applied. The two peaks in doublet subspectra were constrained to have equal areas and widths. Peak areas in sextet subspectra were constrained to the ratio 3:2:1:1:2:3. Because of the strong overlap of the innermost two peaks of sextet subspectra with doublet subspectra, we constrained their positions using the positions of the other 4 peaks and 0.572 for the g-factor ratio of the 14.4 keV excited state to the ground state of ^{57}Fe [e.g., *Gütlich et al.*, 1978].

[13] The combination of reasonable counting statistics and high subspectral area was present for 3 sextets in only two targets; Fe3S3 (assigned to goethite) for the rock Clovis, and Fe3S1 and Fe2.5S1 (assigned to magnetite) for the rock Peace. The Fe3S3 subspectrum was independently fit using a single sextet with skewed-Lorentzian line shape functions [e.g., *Morris et al.*, 1989] and a distribution of sextets having Lorentzian line shapes [e.g., *Rancourt*, 1996]. All other sextet spectra and all doublets were fit using symmetric Lorentzian line shape function. The values of δ, ΔE_Q, B_{hf}, and FWHM for the Fe3S1, Fe2.5S1, and Fe3S3 subspectra of these two targets were used as constraints, together with the area constraint 3:2:1:1:2:3, to fit these subspectra in the spectra of all other targets. The fourth sextet (Fe3S2 assigned to hematite) is present in many targets with reasonable counting statistics and high subspectral area.

[14] The values of δ, ΔE_Q, and FWHM for Fe2D1 (assigned to olivine), Fe2D2 (assigned to pyroxene), and Fe3D1 (assigned to npOx) doublet subspectra were not normally constrained, except for spectra were counting statistics were poor and/or their subspectral areas were small. The Fe3D2 subspectrum (assigned to Fe^{3+} sulfate) occurs in only two samples and with high subspectral area. The Fe2D3 subspectrum (assigned to ilmenite) was not substantial in any sample, so that its MB parameters are known with less certainty.

[15] The values of the MB parameters δ, ΔE_Q, B_{hf}, and FWHM for individual targets that were derived from least squares fits, or were used in the computations as constraints, are given in Table 1 (Fe2D1, Fe2D2, and Fe3D1 subspectra), Table 2 (Fe2D3 and Fe3D2 subspectra), and Table 3 (all sextet subspectra). The spectrum used in each computation is the sum over the temperature interval given in the last column of each table. Parameters in square brackets are constraints. MB parameters for Fe2D1 and Fe2D2 subspectra averaged over specific classes of rocks and soils are in

Table 1. Mössbauer Parameters δ, ΔE_Q, and FWHM for Fe2D1 (Ol), Fe2D2 (Px), and Fe3D1 (npOx) Doublets[a]

	Fe2D1 (Ol)			Fe2D2 (Px)			Fe3D1 (npOx)			
Generic Name (Assignment)	δ, mm/s	ΔE_Q, mm/s	FWHM, mm/s	δ, mm/s	ΔE_Q, mm/s	FWHM, mm/s	δ, mm/s	ΔE_Q, mm/s	FWHM, mm/s	T, K
A014SU0 (FirstSoil)[b]	1.16[c]	2.98	0.39	1.15	2.11	0.54	0.35	0.96	0.71	230–280
A018RU0 (Adirondack_Blue)	1.15	3.00	0.42	1.15	2.07	0.45	0.40	0.87	0.49	210–240
A033RB0 (Adirondack_Blue)	1.16	2.96	0.38	1.16	2.04	0.48	0.41	0.84	0.44	230–270
A034RR0 (Adirondack_Blue)	1.15	2.94	0.38	1.15	2.04	0.46	0.38	0.85	0.38	220–270
A042RU0 (MimiShoe_Lace)	1.15	2.95	0.37	1.17	2.05	0.45	0.38	0.79	0.57	240–270
A043SD0 (MimiTracks_Middle)	1.15	3.02	0.39	1.14	2.12	0.50	0.39	0.77	0.67	200–220
A047SU0 (LagunaHollow_Trout1)	1.15	2.96	0.41	1.14	2.08	0.47	0.40	0.79	0.67	200–260
A049ST2 (LagunaHollow_Floor3)	1.15	2.97	0.37	1.15	2.12	0.53	0.42	0.86	0.73	210–270
A050ST1 (LagunaHollow_WallMIonly)	1.15	2.98	0.38	1.14	2.11	0.56	0.40	0.85	0.65	210–280
A058RU0 (Humphrey_AshleyJ)	1.16	3.01	0.39	1.15	2.11	0.51	0.38	0.76	0.66	210–260
A059RB0 (Humphrey_Heyworth1)	1.16	3.00	0.38	1.16	2.10	0.51	0.38	0.75	0.66	210–260
A060RR0 (Humphrey_Heyworth2)	1.16	3.02	0.40	1.16	2.07	0.50	0.35	0.79	0.44	210–260
A069SU0 (Desert_Gobi)	1.16	3.00	0.37	1.16	2.13	0.54	0.37	0.90	0.76	210–270
A073SD0 (BearPaw_Panda)	1.16	3.00	0.38	1.15	2.11	0.53	0.38	0.84	0.62	200–270
A076RU0 (PaperBack_Appendix)	1.15	2.97	0.44	1.16	2.03	0.49	0.36	0.88	0.53	220–250
A077SU0 (MazatzalFlats_Soil1)	1.15	2.97	0.44	1.16	2.02	0.52	[0.37][d]	0.86	[0.66]	230–250
A079RU0 (Mazatzal_NewYork)	1.16	3.03	0.38	1.17	2.10	0.53	0.37	0.84	0.64	200–250
A080RB0 (Mazatzal_NewYork)	1.16	3.02	0.41	1.16	2.08	0.45	0.37	0.83	0.64	200–250
A082RR0 (Mazatzal_NewYork)	1.16	3.01	0.39	1.16	2.07	0.47	0.35	0.82	0.54	210–250
A083RU0 (Mazatzal_Oregon)	1.14	3.00	0.36	1.14	2.08	0.50	0.37	0.80	0.63	200–250
A084RR0 (Mazatzal_Brooklyn)	1.15	2.98	0.39	1.14	2.05	0.47	0.36	0.85	0.53	210–250
A094RU0 (Route66_Candidate7)	[1.16]	[3.01]	[0.40]	[1.16]	[2.08]	[0.48]	[0.38]	[0.99]	[0.59]	230–260
A100RB0 (Route66_SoHo)	1.16	3.01	0.40	1.16	2.08	0.48	0.38	0.99	0.59	200–250
A110SU0 (WaffelFlats_Soil1)	1.14	2.92	0.38	1.13	2.09	0.44	[0.37]	0.82	0.79	230–250
A113ST1 (BigHole_MayFly)	1.15	3.00	0.41	1.15	2.16	0.48	[0.37]	0.84	0.79	230–250
A114ST2 (Bighole_RS2)	1.14	2.95	0.45	1.14	2.06	[0.49]	[0.37]	0.79	0.83	230–260
A122SD0 (Cutthroat_Owens)	[1.16]	[3.00]	[0.37]	[1.16]	[2.13]	[0.54]	[0.37]	[0.90]	[0.77]	230–250
A135SD0 (MountHillyer_HorseFlats)	1.17	2.95	0.36	1.15	2.10	0.55	[0.37]	0.90	0.76	240–260
A140ST1 (Boroughs_MillBasin)	1.14	2.97	0.37	1.15	2.10	0.53	0.37	0.87	0.66	230–250
A141ST2 (Boroughs_HellsKitchen)	1.16	2.95	0.37	1.16	2.09	0.51	0.38	0.91	0.63	240–260
A150RU0 (Mohave_Joshua)	1.15	2.96	0.37	1.16	2.08	0.45	0.39	0.85	0.53	230–260
A158SD0 (Shreaded_Dark4)	1.15	2.99	0.37	1.15	2.12	0.57	[0.37]	0.87	0.71	230–250
A161RU0 (EndofRainbow_DantesPeak)	[1.16]	[3.02]	[0.42]	1.17	2.21	0.43	0.38	0.91	0.75	210–240
A164RU0 (EndofRainbow_Goldklumpen)	[1.16]	[3.02]	[0.42]	1.18	2.23	0.44	0.36	0.98	0.68	210–240
A166RU0 (FortKnox_Goldbar)	[1.16]	[3.02]	[0.42]	1.18	2.19	0.44	0.36	0.94	0.66	220–250
A167SU0 (Goldfinger_Jaws)	1.16	3.01	0.35	1.15	2.16	0.58	0.34	0.95	0.81	230–250
A171RR0 (PotOfGold_FoolsGold)	[1.16]	[3.02]	[0.42]	1.17	2.17	0.47	[0.36]	1.04	0.60	190–250
A173RR0 (HanksHollow_PotOfGold)	[1.16]	[3.02]	[0.42]	1.16	2.22	0.46	0.40	0.92	0.64	190–250
A176RU0 (Breadbox_Sourdough)	[1.16]	[3.02]	[0.42]	1.13	2.14	0.51	[0.40]	[0.90]	[0.58]	190–250
A178RU0 (StringofPearls_Pearl)	[1.16]	[3.02]	[0.42]	1.16	2.17	0.47	0.36	1.01	0.75	190–250
A182SU0 (CookieCutter_Shortbread)	1.15	2.98	0.38	1.16	2.12	0.54	0.37	0.83	0.72	240–260
A193RU0 (WoolyPatch_Mammoth4)	[1.15]	[2.99]	[0.42]	1.16	2.14	0.44	0.33	0.88	0.62	230–260
A194RU0 (WoolyPatch_Sabre)	[1.15]	[2.99]	[0.42]	1.16	2.15	0.37	0.36	0.86	0.66	210–230
A198RR0 (WoolyPatch_Sabre)	[1.15]	[2.99]	[0.42]	1.17	2.16	0.43	0.37	0.91	0.70	200–230
A200RR0 (WoolyPatch_Mastadon)	[1.15]	[2.99]	[0.42]	1.17	2.17	0.45	0.36	0.88	0.67	200–220
A213RU0 (Clovis_Plano)	[1.16]	[3.02]	[0.42]	[1.16]	2.21	0.65	0.37	1.04	0.74	210–250
A215RB0 (Clovis_Plano)	[1.16]	[3.02]	[0.42]	[1.16]	2.19	0.61	0.37	1.03	0.72	210–250
A218RR0 (Clovis_Plano)	[1.16]	[3.02]	[0.42]	[1.16]	2.30	0.69	0.39	1.02	0.72	210–260
A230RU0 (Ebenezer_Cratchit)	[1.15]	[2.99]	[0.42]	[1.16]	2.38	0.72	0.36	1.09	0.69	210–230
A233RR0 (Ebenezer_Ratchit2)	[1.15]	[2.99]	[0.42]	[1.16]	2.49	0.57	0.38	1.07	0.79	200–230
A260SD0 (Conjunction_Disturbance)	1.15	3.01	0.40	1.15	2.10	0.56	0.37	0.85	0.67	210–250
A269RU0 (Temples_Dwarf)	[1.16]	[3.02]	[0.42]	[1.16]	2.22	0.70	0.37	0.99	0.77	210–240
A275RU0 (Tetl_Clump)	[1.16]	[3.02]	[0.42]	[1.16]	2.17	0.82	0.37	0.99	0.67	210–250
A281SD0 (TakeaBreak_Coffee)	1.15	3.00	0.39	1.15	2.12	0.54	0.34	0.98	0.67	210–250
A285RU0 (Uchben_Koolik)	[1.16]	[3.02]	[0.42]	[1.16]	2.26	0.70	0.37	1.00	0.74	210–240
A288RR0 (Uchben_Koolik)	[1.16]	[3.02]	[0.42]	[1.16]	2.42	0.58	0.38	1.03	0.76	210–240
A299RU0 (Lutefisk_Twins)	[1.16]	[3.02]	[0.42]	[1.16]	[2.21]	[0.61]	[0.36]	[1.00]	[0.66]	210–260
A302RB0 (Lutefisk_FlatFish)	[1.16]	[3.02]	[0.42]	[1.16]	2.24	0.63	0.36	1.04	0.70	210–260
A303RB0 (Lutefisk_Roe)	[1.16]	[3.02]	[0.42]	[1.16]	2.22	0.62	0.36	0.97	0.62	210–260
A316SD0 (Yams_Turkey)	1.15	2.98	0.40	1.14	2.12	0.56	0.39	0.83	0.72	210–260
A336RR0 (Wishstone_Chisel)	1.18	2.97	0.41	1.18	2.14	0.45	0.39	0.95	0.75	210–250
A342SD0 (Penny_DS1)	1.16	3.02	0.40	1.15	2.12	0.54	0.37	0.94	0.70	210–260
A350RU0 (WishingWell_Dreaming)	1.16	2.98	0.35	1.17	2.15	0.48	0.37	0.97	0.60	210–260
A353RU0 (Champagne_Lip)	[1.16]	[2.93]	[0.43]	1.16	[2.05]	[0.39]	[0.35]	[0.90]	[0.60]	210–250
A358RR0 (Champagne_RAT2)	1.16	2.93	0.42	1.17	2.07	0.30	0.37	0.94	0.62	210–250
A376RR0 (Peace_Justice1)	1.14	3.04	0.36	1.15	2.16	0.41	0.35	0.91	0.60	210–250
A379RR0 (Peace_Justice2)	1.14	3.05	0.37	1.15	2.14	0.44	0.37	0.89	0.56	210–250
A385RB0 (Alligator_Jambalaya)	1.15	3.05	0.37	1.16	2.17	0.42	0.35	0.92	0.64	210–260
A401SD0 (Pasadena_PasoRobles)	[1.15]	[2.95]	[0.38]	[1.16]	[2.17]	[0.56]	–	–	–	190–280
A418RR0 (WatchTower_Joker)	–	–	–	–	–	–	0.37	1.01	0.66	200–270
A426SD0 (PasoRobles2_PasoDark)	1.14	2.96	0.39	1.15	2.13	0.56	–	–	–	250–280

Table 1. (continued)

Generic Name (Assignment)	Fe2D1 (Ol) δ, mm/s	Fe2D1 (Ol) ΔE_Q, mm/s	Fe2D1 (Ol) FWHM, mm/s	Fe2D2 (Px) δ, mm/s	Fe2D2 (Px) ΔE_Q, mm/s	Fe2D2 (Px) FWHM, mm/s	Fe3D1 (npOx) δ, mm/s	Fe3D1 (npOx) ΔE_Q, mm/s	Fe3D1 (npOx) FWHM, mm/s	T, K
A429SD0 (PasoRobles2_PasoLight1)	[1.15]	[2.95]	[0.38]	1.16	[2.17]	[0.56]	–	–	–	200–280
A459SU0 (Crumble_Almonds)	1.15	3.00	0.39	1.14	2.12	0.57	[0.37]	0.95	0.78	200–270
A472RB0 (Keystone_Haunch)	–	–	–	1.16	2.19	0.46	0.35	0.89	0.71	210–270
A479SU0 (Liberty_Bell)	1.15	3.00	0.39	1.15	2.17	0.51	0.40	0.86	0.70	200–260
A483RU0 (Keel_Reef)	1.15	3.06	0.36	1.14	2.23	0.45	0.35	0.91	0.77	200–270
A483RU0 (Keel_Davis)	[1.15]	[3.01]	[0.38]	1.17	2.17	0.39	0.37	0.87	0.75	210–270
A493RB0 (LarrysLookout_Paros)	[1.15]	[3.01]	[0.38]	1.16	[2.20]	[0.46]	0.36	1.02	0.68	200–280
A498RU0 (Pequod_Ahab)	[1.15]	[3.01]	[0.38]	1.16	[2.20]	[0.46]	0.36	0.99	0.70	210–270
A501RU0 (Pequod_MobyDick)	[1.15]	[3.01]	[0.38]	1.16	[2.20]	[0.46]	0.37	1.01	0.70	210–270
A502SU0 (Pequod_Doubloon)	1.16	3.01	0.36	1.16	2.20	0.47	0.35	0.83	0.97	210–270
A510RB0 (Backstay_Scuppler)	1.15	3.00	0.39	1.16	2.12	0.43	0.34	0.90	0.59	210–270
Average MB Parameters for Spectra From Individual Targets Summed Over the Temperature Range in the Last Column										
Average all measurements	1.15	2.99	0.39	1.16	2.15	0.51	0.37	0.91	0.67	
Standard deviation (2σ)	0.02	0.06	0.04	0.02	0.16	0.17	0.03	0.16	0.18	
Average MB Parameters for Spectra Summed Over Narrow Temperature Intervals										
Average	1.15	2.99	0.39	1.16	2.14	0.51	0.37	0.91	0.67	
Standard deviation (2σ)	0.02	0.04	0.04	0.02	0.14	0.17	0.04	0.14	0.18	

[a]Parameters were calculated from spectra summed over the temperature interval given in the last column. The values of δ are referenced to metallic iron foil at the same temperature as the sample.

[b]Target naming convention: Awwwxyz (Feature-name_Target-name). A = MER-A (Gusev crater); www = Gusev crater sol number that data product was returned to Earth. For integrations covering multiple sols, the sol of the first returned data product is used. x = R (rock) or S (soil); y = U (undisturbed), D (disturbed), T (trench), B (RAT-brushed surface), R (RAT-ground surface), or G (RAT grindings); z = 0 by default; z = 1, 2, 3... for multiple analyses of the same target on the same sol. For AxxxSTz, z = 1, 2, 3... with increasing number corresponding to increasing depth. Alphanumeric strings before parentheses are unique target identifiers.

[c]Unless otherwise stated, MB parameter uncertainty is ±0.02 mm/s.

[d]MB parameters in brackets are constraints used in the fitting procedure.

Table 4. The subspectral areas obtained from the fitting procedure are compiled in Table 5. The areas include a correction factor (the *f*-factor) to account for differences in recoil-free fractions ($f(Fe^{3+})/f(Fe^{2+})$ = 1.21 independent of mineralogical composition [*De Grave and Van Alboom*, 1991; *Morris et al.*, 1995]).

3. Phase Identification

3.1. Overview

[16] We used three approaches for identification of Fe-bearing phases in Gusev Mössbauer spectra: (1) literature databases of Mössbauer parameters, (2) correlation of subspectral areas, and (3) data sets from other MER instruments.

3.1.1. Literature Databases

[17] There are a number of compilations of Mössbauer parameters (δ, ΔE_Q, and B_{hf}) for known mineralogical compositions that can be used to infer mineralogical compositions from the corresponding parameters derived from MER MB spectra [e.g., *Burns and Solberg*, 1990; *McCammon*, 1995; *Stevens et al.*, 1998; *de Souza*, 1999]. Typically, these compilations have data for measurements near room (~295 K), liquid nitrogen (~77 K), and liquid helium (4 K) temperatures. MER MB spectra were acquired

Table 2. Mössbauer Parameters δ, ΔE_Q, and FWHM for Ilmenite and Fe^{3+}-Sulfate Doublets[a]

Generic Name (Assignment)	Fe2D3 (Ilm) δ, mm/s	Fe2D3 (Ilm) ΔE_Q, mm/s	Fe2D3 (Ilm) FWHM, mm/s	Fe3D2 (Fe^{3+}-Sulfate) δ, mm/s	Fe3D2 (Fe^{3+}-Sulfate) ΔE_Q, mm/s	Fe3D2 (Fe^{3+}-Sulfate) FWHM, mm/s	T, K
A336RR0 (Wishstone_Chisel)	1.07[b]	.70	0.44	–	–	–	210–250
A350RU0 (WishingWell_Dreaming)	[1.07][c]	[0.70]	[0.44]	–	–	–	210–260
A353RU0 (Champagne_Lip)	[1.07]	[0.70]	[0.44]	–	–	–	210–250
A358RR0 (Champagne_RAT2)	1.05	0.74	[0.32]	–	–	–	210–250
A401SD0 (Pasadena_PasoRobles)	–	–	–	0.42	0.62	0.60	190–280
A418RR0 (WatchTower_Joker)	[1.07]	0.82	[0.44]	–	–	–	200–270
A429SD0 (PasoRobles2_PasoLight1)	–	–	–	0.43	0.55	0.68	200–280
A472RB0 (Keystone_Haunch)	[1.07]	[0.70]	[0.44]	–	–	–	210–270
A483RU0 (Keel_Reef)	[1.07]	[0.70]	[0.44]	–	–	–	200–270
A486RB0 (Keel_Davis)	1.08	0.89	0.34	–	–	–	210–270
A498RU0 (Pequod_Ahab)	1.07	0.76	[0.32]	–	–	–	210–270
A501RU0 (Pequod_MobyDick)	1.06	0.85	[0.32]	–	–	–	210–270
A502SU0 (Pequod_Doubloon)	1.05	0.79	0.41	–	–	–	210–270
A510RB0 (Backstay_Scupper)	[1.07]	0.85	0.32	–	–	–	210–270
Average all measurements	1.07	0.80	0.38	0.43	0.58	0.64	
Standard deviation (1σ)	0.01	0.06	0.07	0.02	0.05	0.06	

[a]Parameters were calculated from spectra summed over the temperature interval given in the last column. Values of δ are with respect to metallic iron foil at the same temperature as the sample.

[b]Unless otherwise stated, MB parameter uncertainties are ±0.03 mm/s for Fe2D3 and ±0.02 mm/s for Fe3D2.

[c]MB parameters in brackets are constraints used in the fitting procedure.

Table 3. Mössbauer Parameters δ, ΔE_Q, and B_{hf} for Sextets[a]

	Sextet 1			Sextet 2			
	δ, mm/s	ΔE_Q, mm/s	B_{hf}, mm/s	δ, mm/s	ΔE_Q, mm/s	B_{hf}, mm/s	T, K
Sextet 1 = Fe3S1 (Magnetite, tet-Fe^{3+}); Sextet 2 = Fe2.5S1 (Magnetite, oct-$Fe^{2.5+}$)							
A379RR0 (Peace_Justice2)	0.31[b]	0.06	50.1	0.64	0.00	46.9	210–250
All other Mt-bearing targets	[0.31][c]	[0.06]	[50.1]	[0.64]	[0.00]	[46.9]	
Fe3S3 (Goethite, oct-Fe^{3+})							
A213RU0 (Clovis_Plano)	0.38	−0.14	36.5	–	–	–	210–250
A215RB0 (Clovis_Plano)	0.37	−0.20	36.4	–	–	–	210–250
A218RR0 (Clovis_Plano)	0.38	−0.15	36.7	–	–	–	210–260
All other Gt-bearing targets	[0.38]	[−0.17]	[36.5]	–	–	–	–
Sextet 1 = Fe3S2 (Hematite, oct-Fe^{3+}, $\Delta E_Q < 0$); Sextet 2 = Fe3S2 (Hematite, oct-Fe^{3+}, $\Delta E_Q > ; 0$)							
All Laguna Class Soil	[0.37]	[−0.16]	[51.7]	–	–	–	–
All Adirondack Class Rock	[0.37]	[−0.16]	[51.7]	–	–	–	–
A161RU0 (EndofRainbow_DantesPeak)	0.37	−0.18	52.4	0.37	0.26	53.6	210–240
A164RU0 (EndofRainbow_Goldklumpen)	0.34	−0.20	52.2	0.38	0.32	53.9	210–240
A166RU0 (FortKnox_Goldbar)	0.37	−0.15	52.1	–	–	–	220–250
A171RR0 (PotOfGold_FoolsGold)	[0.37]	−0.24	52.1	[0.37]	0.37	53.2	190–250
A173RR0 (HanksHollow_PotOfGold)	0.38	−0.15	52.0	0.38	0.30	53.8	190–250
A176RU0 (BreadBox_Sourdough)	–	–	–	0.34	0.03	52.4	190–250
A178RU0 (StringofPearls_Pearl)	0.36	−0.01	51.8	0.40	0.23	54.1	190–250
A193RU0 (WoolyPatch_Mammoth4)	[0.37]	−0.19	51.5	–	–	–	230–260
A194RU0 (WoolyPatch_Sabre)	0.34	−0.11	52.5	–	–	–	210–230
A198RR0 (WoolyPatch_Sabre)	0.39	−0.18	51.8	–	–	–	200–230
A200RR0 (WoolyPatch_Mastadon)	0.38	−0.18	52.0	–	–	–	200–220
A213RU0 (Clovis_Plano)	0.38	−0.07	52.6	–	–	–	210–250
A215RB0 (Clovis_Plano)	0.36	−0.04	52.5	–	–	–	210–250
A218RR0 (Clovis_Plano)	0.38	−0.09	52.3	–	–	–	210–260
A230RU0 (Ebenezer_Cratchit)	0.37	−0.01	52.5	–	–	–	210–230
A233RR0 (Ebenezer_Ratchit2)	0.39	−0.13	52.0	–	–	–	200–230
A269RU0 (Temples_Dwarf)	0.36	−0.14	52.7	–	–	–	210–240
A275RU0 (Tetl_Clump)	0.40	−0.05	51.7	–	–	–	210–250
A285RU0 (Uchben_Koolik)	–	–	–	0.38	0.06	52.8	210–240
A288RR0 (Uchben_Koolik)	–	–	–	0.37	0.00	52.6	210–240
A299RU0 (Lutefisk_Twins)	[0.37]	[−0.13]	[52.3]	–	–	–	210–260
A302RB0 (Lutefisk_FlatFish)	0.38	−0.10	51.6	–	–	–	210–260
A303RB0 (Lutefisk_Roe)	0.38	−0.15	52.1	–	–	–	210–260
A336RR0 (Wishstone_Chisel)	0.34	−0.14	52.8	–	–	–	210–250
A350RU0 (WishingWell_Dreaming)	0.38	−0.22	52.6	–	–	–	210–260
A353RU0 (Champagne_Lip)	[0.34]	[−0.14]	[52.8]	–	–	–	210–250
A358RR0 (Champagne_RAT2)	[0.34]	[−0.14]	[52.8]	–	–	–	210–250
A401SD0 (Pasadena_PasoRobles)	0.39	−0.16	51.3	0.36	0.05	53.4	190–280
A418RR0 (WatchTower_Joker)	–	–	–	0.38	0.16	53.4	200–270
A429SD0 (PasoRobles2_PasoLight1)	–	–	–	[0.37]	[0.02]	[52.9]	200–280
A472RU0 (Keystone_Haunch)	0.39	−0.17	51.5	–	–	–	210–270
A483RU0 (Keel_Reef)	0.38	−0.03	51.9	0.36	0.21	53.5	200–270
A486RB0 (Keel_Davis)	0.39	−0.07	51.7	0.36	0.18	53.3	210–270
A493RB0 (LarrysLookout_Paros)	0.39	−0.15	51.5	0.33	0.21	53.4	200–280
A498RU0 (Pequod_Ahab)	0.38	−0.04	52.9	–	–	–	210–270
A501RU0 (Pequod_MobyDick)	–	–	–	0.39	0.05	52.5	210–270
A502SU0 (Pequod_Doubloon)	0.35	−0.14	52.8				210–270
A510RB0 (Backstay_Scupper)	–	–	–	[0.369]	[0.173]	[53.13]	210–270
Average Hm all measurements	0.37	−0.13	52.2	0.37	0.25	53.6	
Standard deviation (1σ)	0.02	0.06	0.5	0.02	0.07	0.3	

[a]Parameters were calculated from spectra summed over the temperature interval given in the last column. Values of δ are with respect to metallic iron foil at the same temperature as the sample.
[b]MB parameter errors are ±0.02 mm/s for δ and ΔE_Q and ±0.8 T for B_{hf}.
[c]MB parameters in brackets are constraints used in the fitting procedures.

over the Martian diurnal temperature range (180–300 K), and the different measurement temperatures could obviate direct use of available literature data if the Mössbauer parameters are strongly dependent on temperature. On the basis of the following discussion, room temperature literature data can generally be used to constrain the mineralogical composition of Fe-bearing phases in MER MB spectra.

[18] The typical instrument configuration in laboratory experiments, where the temperature dependence of MB parameters is determined, is to control the sample (absorber) temperature in a cryostat or oven and to have the source and velocity drive at room temperature. Because the sample and source are at different temperatures, there is a large temperature dependence measured for δ when its value as a function of temperature is reported with respect to the value for some standard at room temperature (normally the center position of the spectrum of metallic iron foil). For the MER MB instrument [*Klingelhöfer et al.*, 2003], the difference in

Table 4. Average Mössbauer Parameters δ and ΔE_Q and Their Standard Deviations for Ol and Px for Classes and Subclasses of Rock and Soil[a]

	Px (Fe2D2)				Ol (Fe2D1)			
	δ		ΔE_Q		δ		ΔE_Q	
	Ave., mm/s	Std.Dev., mm/s	Ave., mm/s	Std.Dev., mm/s	Ave., mm/s	Std.Dev., mm/s	Ave., mm/s	Std.Dev., mm/s
Rocks								
Adirondack Class	1.15	0.02	2.06	0.03	1.16	0.02	2.99	0.03
Joshua Subclass	1.16	0.02	2.06	0.03	1.15	0.02	2.96	0.02
Wishstone Class	1.17	0.02	2.12	0.04	1.17	0.02	2.97	0.03
Backstay Class	1.16	0.02	2.12	0.02	1.15	0.02	3.00	0.02
WoolyPatch Subclass	1.17	0.02	2.15	0.02	–	–	–	–
Peace Class	1.16	0.02	2.16	0.02	1.15	0.02	3.05	0.02
PotOfGold Subclass	1.16	0.02	2.18	0.03	–	–	–	–
Keystone Subclass	1.16	0.02	2.19	0.02	–	–	–	–
Keel Subclass	1.15	0.02	2.20	0.04	–	–	–	–
Clovis Subclass	na	na	2.27	0.10	–	–	–	–
Soils								
Boroughs Subclass	1.15	0.02	2.09	0.02	1.15	0.02	3.01	0.02
Gobi Subclass	1.15	0.02	2.10	0.02	1.15	0.02	2.97	0.02
Liberty Subclass	1.15	0.02	2.11	0.05	1.15	0.02	2.98	0.02
Panda Subclass	1.15	0.02	2.12	0.02	1.15	0.02	3.00	0.02

[a]Values of δ are with respect to metallic iron foil at the same temperature as the sample. Table rows are ordered by increasing ΔE_Q for Px.

temperature between the emitter (the Martian surface), the ^{57}Co source, and the metallic iron foil calibration standard is <10 K, so that values of δ are measured and reported with respect to metallic iron foil at nominally the sample temperature. Thus, contrary to the discussion of *Dyar and Schaefer* [2004], room temperature literature data for δ can be directly compared to corresponding MER MB data because the difference in temperature between source and sample is ~0 K in both cases. We will show later that δ is not dependent on temperature within experimental uncertainty for MER MB spectra.

[19] For Fe-bearing phases characterized by paramagnetic doublets over the temperature range 180–295 K (e.g., olivine, pyroxene, and ilmenite), ΔE_Q is not strongly dependent on temperature, as we will show later for MER MB spectra. Both ΔE_Q and B_{hf} can be strongly dependent on temperature for Fe-bearing phases characterized by magnetic sextets (e.g., hematite, goethite, and magnetite), particularly if the Néel or Curie temperature are proximate to the measurement temperature or a magnetic transition occurs. The phase that is both present in many MER spectra and has significant temperature dependence for ΔE_Q and B_{hf} at Martian diurnal temperatures is hematite, which undergoes a magnetic transition (Morin transition) near 260 K for pure, well-crystalline, bulk hematite. The temperature of the Morin transition, the temperature interval over which it occurs, and the magnitude of the change in ΔE_Q and B_{hf} with temperature vary from sample to sample, depending on the chemical purity, crystallinity, and/or particle size of the hematite [e.g., *Bando et al.*, 1965; *Murad and Johnston*, 1987; *De Grave and Vandenberghe*, 1990; *Dang et al.*, 1998]. Goethite and magnetite do not undergo magnetic transitions at Martian diurnal surface temperatures.

[20] In summary, the ideal database for constraining the mineralogical composition of Martian Fe-bearing phases is one where measurements are made at diurnal surface temperatures with a MER-like instrument where the ^{57}Co source, metallic iron foil calibration standard, and sample are all at the same temperature. However, such a database is not required to constrain the mineralogical composition of Martian Fe-bearing phases. Mössbauer parameters for paramagnetic doublets obtained from laboratory measurements near room temperature are applicable at Martian diurnal temperatures. For magnetic sextets, the Mössbauer parameters for geologically important phases (e.g., magnetite, hematite, and goethite) have previously been measured at Martian diurnal temperatures as a consequence of studying the magnetic properties of these phases. Although there is a large amount of data in the Mössbauer literature that can be used for mineralogical assignment of subspectra in MER MB spectra, it is important to remember there may be Fe-bearing phases on Mars that are unknown in terrestrial natural and synthetic samples.

3.1.2. Correlation of Subspectral Areas

[21] As Spirit traverses over the Martian surface, measurements are made at regular intervals by all Athena science instruments. It often happens that a number of MB spectra in a traverse segment can be characterized as having different relative proportions of the same components, i.e., only subspectral areas vary from target-to-target. This information, together with images and analytical data from the other science instruments, define geologic units and boundaries. MB measurements on targets that have different proportions of the same components also provide a way to constrain the mineralogical composition of the components. For example, a positive correlation of areas of two subspectra could be evidence that the subspectra are derived from different Fe sites in the same Fe-bearing phase. Correlations involving MB subspectral areas and APXS elemental chemistry can also be used to constrain mineralogical compositions. For example, a positive correlation of a subspectral area with the concentration of some element might imply that the element and subspectrum-Fe are in the same phase.

3.1.3. Other MER Data Sets

[22] Mineralogical assignments made on the basis of MB spectra and data from the other Athena science instruments, particularly APXS, Mini-TES, and Pancam multispectral

Table 5. Mössbauer Areas for Component Subspectra (f-Factor Corrected), Fe^{3+}/Fe_T, and Temperature Measurement Interval for Mössbauer Spectra of Gusev Crater Rock and Soil Targets

Subspectrum Generic Name Phase Assignment	Fe2D1 Ol, %	Fe2D2 Px, %	Fe2D3 Ilm, %	Fe3D1 npOx, %	Fe3D2 Sulfate, %	Mt, %	Fe3S1 Mt(tet), %	Fe2.5S1 Mt(oct), %	Fe3S2 Hm, %	Fe3S3 Gt, %	Total, %	Fe^{3+}/Fe_T	T, K
Plains, Gusev Crater													
A014SU0 (FirstSoil)	34[a]	35	0	23	0	6	3	3	2	0	100	0.29[b]	230–280
A018RU0 (Adirondack_Blue)	47	32	0	7	0	13	7	7	1	0	100	0.18	210–240
A033RB0 (Adirondack_Blue)	46	33	0	7	0	13	5	8	1	0	100	0.17	230–270
A034RR0 (Adirondack_Blue)	48	32	0	6	0	13	6	7	1	0	100	0.16	220–270
A042RU0 (MimiShoe_Lace)	28	23	0	19	0	26	13	14	4	0	100	0.43	240–270
A043SD0 (MimiTracks_Middle)	38	32	0	16	0	8	3	6	6	0	100	0.27	200–220
A047SU0 (LagunaHollow_Trout1)	36	31	0	20	0	9	3	7	4	0	100	0.30	200–260
A049ST2 (LagunaHollow_Floor3)	38	37	0	15	0	9	4	5	1	0	100	0.23	210–270
A050ST1 (LagunaHollow_WallMIonly)	38	37	0	15	0	8	4	5	1	0	100	0.23	210–280
A058RU0 (Humphrey_AshleyJ)	43	35	0	8	0	11	4	7	3	0	100	0.18	210–260
A059RB0 (Humphrey_Heyworth1)	43	35	0	8	0	12	6	6	2	0	100	0.19	210–260
A060RR0 (Humphrey_Heyworth2)	50	32	0	6	0	11	6	5	1	0	100	0.15	210–260
A069SU0 (Desert_Gobi)	30	33	0	28	0	7	4	3	2	0	100	0.36	210–270
A073SD0 (BearPaw_Panda)	37	35	0	13	0	12	6	6	3	0	100	0.25	200–270
A076RU0 (PaperBack_Appendix)	41	36	0	19	0	3	3	1	0	0	100	0.23	220–250
A077SU0 (MazatzalFlats_Soil1)	39	26	0	19	0	13	5	8	3[c]	0	100	0.30	230–250
A079RU0 (Mazatzal_NewYork)	35	26	0	29	0	5	3	2	4	0	100	0.37	200–250
A080RB0 (Mazatzal_NewYork)	40	22	0	28	0	5	2	3	4	0	100	0.36	200–250
A082RR0 (Mazatzal_NewYork)	49	31	0	12	0	6	4	2	2	0	100	0.18	210–250
A083RU0 (Mazatzal_Oregon)	28	20	0	40	0	6	3	3	6	0	100	0.50	200–250
A084RR0 (Mazatzal_Brooklyn)	57	32	0	5	0	6	3	3	0	0	100	0.10	210–250
A094RU0 (Route66_Candidate7)	53	36	0	10	0	2	1	1	0	0	100	0.11	230–260
A100RB0 (Route66_SoHo)	57	37	0	7	0	0	0	0	0	0	100	0.07	200–250
A110SU0 (WaffelFlats_Soil1)	30	23	0	25	0	22	9	13	0	0	100	0.40	230–250
A113ST1 (BigHole_MayFly)	41	30	0	18	0	11	5	5	0	0	100	0.26	230–250
A114ST2 (Bighole_RS2)	28	27	0	37	0	8	5	3	1	0	100	0.44	230–260
A122SD0 (Cutthroat_Owens)	32[d]	32[c]	0	23	0	11[c]	7[c]	4	2	0	100	0.34	230–250
A135SD0 (MountHillyer_HorseFlats)	34	38	0	18	0	9	4	5	2	0	100	0.26	240–260
A140ST1 (Boroughs_MillBasin)	30	31	0	29	0	8	3	4	2	0	100	0.36	230–250
A141ST2 (Boroughs_HellsKitchen)	27	29	0	34	0	9	5	5	1	0	100	0.42	240–260
A150RU0 (Mohave_Joshua)	33	37	0	11	0	17	8	9	2	0	100	0.26	230–260
West Spur, Columbia Hills, Gusev Crater													
A158SD0 (Shreaded_Dark4)	38	38	0	16	0	6	4	3	1	0	100	0.22	230–250
A161RU0 (EndofRainbow_DantesPeak)	9	34	0	15	0	3	0	3	39	0	100	0.56	210–240
A164RU0 (EndofRainbow_Goldklumpen)	1	36	0	21	0	2	0	2	41	0	100	0.62	210–240
A166RU0 (FortKnox_Goldbar)	10	37	0	13	0	2	0	2	38	0	100	0.52	220–250
A167SU0 (Goldfinger_Jaws)	39	33	0	17	0	10	5	4	2	0	100	0.26	230–250
A171RR0 (PotOfGold_FoolsGold)	10	38	0	15	0	5	3	3	32	0	100	0.51	190–250
A173RR0 (HanksHollow_PotOfGold)	1	36	0	12	0	2	0	2	49	0	100	0.62	190–250
A176RU0 (Breadbox_Sourdough)	14	37	0	11	0	6	4	2	31	0	100	0.47	190–250
A178RU0 (StringofPearls_Pearl)	19	37	0	13	0	4	0	3	27	0	100	0.43	190–250
A182SU0 (CookieCutter_Shortbread)	25	36	0	25	0	11	7	3	4	0	100	0.38	240–260
A193RU0 (WoolyPatch_Mammoth4)	4	49	0	18	0	12	11	2	12	4	100	0.46	230–260
A194RU0 (WoolyPatch_Sabre)	6	31	0	29	0	17	9	8	10	7	100	0.59	210–230
A198RR0 (WoolyPatch_Sabre)	2	34	0	25	0	15[c]	7[c]	8	19[d]	3	100	0.59	200–230
A200RR0 (WoolyPatch_Mastadon)	1	33	0	29	0	16	6	9	13	8	100	0.61	200–220
A213RU0 (Clovis_Plano)	2	14[c]	0	27	0	2	1	1	19	35	100	0.83	210–250
A215RB0 (Clovis_Plano)	3	13	0	28	0	1	0	0	20	36	100	0.85	210–250

Table 5. (continued)

Subspectrum Generic Name Phase Assignment	Fe2D1 Ol, %	Fe2D2 Px, %	Fe2D3 Ilm, %	Fe3D1 npOx, %	Fe3D2 Sulfate, %	Mt, %	Fe3S1 Mt(tet), %	Fe2.5S1 Mt(oct), %	Fe3S2 Hm, %	Fe3S3 Gt, %	Total, %	Fe^{3+}/Fe_T	T, K
A218RR0 (Clovis_Plano)	1	14	0	25	0	2	1	1	18	40[c]	100	0.84	210–260
A230RU0 (Ebenezer_Cratchit)	1	15	0	33	0	20	9	11	13	19	100	0.79	210–230
A233RR0 (Ebenezer_Ratchit2)	1	11	0	35	0	19	8	11	14	20	100	0.83	200–230
A260SD0 (Conjunction_Disturbance)	34	33	0	24	0	8	4	4	2	0	100	0.31	210–250
A269RU0 (Temples_Dwarf)	1	22	0	28	0	10	5	5	13	26	100	0.74	210–240
A275RU0 (Tetl_Clump)	2	21	0	23	0	24	10	14	16	15	100	0.70	210–250
A281SD0 (TakeaBreak_Coffee)	30	36	0	20	0	12	6	5	2	0	100	0.31	210–250
A285RU0 (Uchben_Koolik)	2	20	0	33	0	13	5	8	9	24	100	0.74	210–240
A288RR0 (Uchben_Koolik)	2	16	0	38	0	14	6	8	8	22	100	0.79	210–240
A299RU0 (Lutefisk_Twins)	9	25[c]	0	27	0	19	8	11	10	10	100	0.61	210–260
A302RB0 (Lutefisk_FlatFish)	2	23	0	24	0	15	6	9	18	19	100	0.71	210–260
A303RB0 (Lutefisk_Roe)	2	28	0	20	0	20	9	10	12	19	100	0.65	210–260
A316SD0 (Yams_Turkey)	35	33	0	22	0	8	4	4	2	0	100	0.30	210–260
Cumberland Ridge, Husband Hill, Columbia Hills, Gusev Crater													
A336RR0 (Wishstone_Chisel)	20	29	8	16	0	12	7	5	14	0	100	0.40	210–250
A342SD0 (Penny_DS1)	41	33	0	15	0	9	3	6	2	0	100	0.22	210–260
A350RU0 (WishingWell_Dreaming)	29	24	3	19	0	10	6	5	14	0	100	0.41	210–260
A353RU0 (Champagne_Lip)	17[c]	29[d]	4	17	0	10	8	3	7	16[c]	100	0.49	210–250
A358RR0 (Champagne_RAT2)	20	27	7	12	0	9	8	1	11	13	100	0.45	210–250
A376RR0 (Peace_Justice1)	21	28	0	16	0	35	14	22	0	0	100	0.40	210–250
A379RR0 (Peace_Justice2)	24	29	0	14	0	33	13	20	0	0	100	0.37	210–250
A385RB0 (Alligator_Jambalaya)	32	31	0	14	0	23	11	12	0	0	100	0.31	210–260
A401SD0 (Pasadena_PasoRobles)	3	10	0	0	62	5	2	3	20	0	100	0.86	190–280
A418RR0 (WatchTower_Joker)	7	7	3	39	0	1	0	1	31	12	100	0.83	200–270
A426SD0 (PasoRobles2_PasoDark)	30	40	0	19	0	10	4	6	2	0	100	0.27	250–280
A429SD0 (PasoRobles2_PasoLight1)	10	8	0	0	69	6	1	5	7	0	100	0.79	200–280
A459SU0 (Crumble_Almonds)	44	33	0	13	0	8	3	4	3	0	100	0.21	200–270
A472RB0 (Keystone_Haunch)	0	47	6	17	0	10	4	6	15	4	100	0.43	210–270
A479SU0 (Liberty_Bell)	38	34	0	18	0	7	2	5	3	0	100	0.25	200–260
A483RU0 (Keel_Reef)	15	18	1	25	0	10	6	4	31	0	100	0.64	200–270
A486RB0 (Keel_Davis)	4	13	8	27	0	9	3	5	40	0	100	0.73	210–270
A493RB0 (LarrysLookout_Paros)	3	1	2	66	0	0	0	0	18	11	100	0.94	200–280
A498RU0 (Pequod_Ahab)	4	2	6	62	0	0	0	0	14	12	100	0.88	210–270
A501RU0 (Pequod_MobyDick)	7	5	6	55[c]	0	0	0	0	18[c]	9	100	0.82	210–270
A502SU0 (Pequod_Doubloon)	27	26	8	22	0	5	2	3	12	0	100	0.38	210–270
A510RB0 (Backstay_Scuppler)	35	37	3	13	0	11	5	6	2	0	100	0.23	210–270

[a]Uncertainty in subspectral area is ±2% absolute unless otherwise stated.
[b]Uncertainty in Fe^{3+}/Fe_T is ±0.03.
[c]Uncertainty in subspectral area is ±3% absolute.
[d]Uncertainty in subspectral area is ±4% absolute.

data, should as an aggregate be consistent. For example, MB cannot confirm, but is consistent with, the presence of Mg-sulfates inferred from either Mini-TES or APXS data because the MB technique is sensitive only to Fe-bearing phases. Similarly, the presence of Fe-bearing olivine implies detection by both MB and Mini-TES, unless there are detection limit considerations.

3.2. Representative Gusev Mössbauer Spectra

[23] Gusev crater rocks are organized by *Squyres et al.* [2006] into six named classes (Adirondack, Clovis, Peace, Backstay, Wishstone, and Watchtower) plus other rocks on the basis of APXS chemistry [*Gellert et al.*, 2006; *Ming et al.*, 2006]. We added a number of subclasses to the scheme on the basis of diversity of Mössbauer mineralogical compositions within several classes (Figure 1). Also on the basis of APXS chemistry, we organize Gusev crater soils into two named classes (Laguna and PasoRobles) with subclasses plus other soils (Figure 1).

[24] In Figures 2 and 3, we show representative MB spectra for each class and subclass of rock and soil, respectively, along with the component subspectra obtained from the fitting procedures. We were able to describe all Gusev MB spectra with five doublet and four sextet subspectra: three doublets from octahedrally coordinated Fe^{2+} (oct-Fe^{2+}) (Fe2D1, Fe2D2, and Fe2D3), two doublets from octahedrally coordinated Fe^{3+} (oct-Fe^{3+}) (Fe3D1 and Fe3D2), one sextet from tetrahedrally coordinated Fe^{3+} (tet-Fe^{3+}) (Fe3S1), one sextet from coupled oct-Fe^{3+} and oct-Fe^{2+} (Fe2.5S1), and two sextets from oct-Fe^{3+} (Fe3S2 and Fe3S3). The fitting of individual Gusev MB spectra required between three and seven subspectra. Next, we discuss mineralogical assignment of doublet subspectra and then sextet subspectra.

3.3. Mineralogical Assignment of Doublet Subspectra

[25] We show a plot of δ versus ΔE_Q for the subspectra of individual rocks (average values from Table 1) and subclasses of soils in Figure 4. The figure shows that there are at least five different Fe-bearing phases represented by doublets at Gusev crater, assuming each subspectrum is associated with a different phase. Note that for each cluster, the values of δ are nearly the same within error. In contrast, there are significant differences for ΔE_Q, particularly for the Fe3D1 and Fe2D2 doublets. Because the data plotted in this figure were obtained from spectra summed over a range of temperatures (to improve counting statistics), these observations suggest (within each cluster) that δ is not dependent on either temperature or compositional variations and that ΔE_Q is dependent on temperature and/or compositional variations.

3.3.1. Fe2D1, Fe2D2, and Fe3D1

[26] The temperature and compositional dependences of δ and ΔE_Q for the Fe2D1, Fe2D2, and Fe3D1 doublets are investigated in Figure 5. In general, counting statistics in the 10 K wide temperature windows were not adequate to obtain reliable fits. Although we improved the counting statistics by summing adjacent temperature windows (which reduces temperature resolution) and/or by combining multiple analyses of the same or similar rocks and soils (which may compromise mineralogical discrimination), the uncertainties in the calculated values of δ and ΔE_Q are generally larger than they are for the corresponding parameters calculated from spectra summed over all temperature windows. Within measurement error, the values of δ for all three doublets are not dependent on temperature over the range 210–270 K (Figures 5a, 5c, and 5e). For ΔE_Q, there is a clear compositional dependence for the Fe3D1 and Fe2D2 doublets but not the Fe2D1 doublet (Figures 5b, 5d, and 5f). As an example, the values of ΔE_Q for the Fe3D1 doublet for rocks Clovis and Uchben ($\sim$1.00 mm/s) do not overlap within error the corresponding values for the Adirondack Class rocks ($\sim$0.85 mm/s). Similarly, the values of ΔE_Q for the Fe2D2 doublet for the Clovis-Uchben rocks and Adirondack Class ($\sim$2.20–2.30 mm/s and $\sim$2.07 mm/s respectively) are different within measurement error.

[27] The average values and 2σ standard deviations for δ, ΔE_Q, and FWHM from spectra summed over narrow and wide temperature intervals are given at the bottom of Table 1. For each doublet, the averages and standard deviations are essentially identical, implying that the improvement in counting statistics gained by summing data for all temperature windows has not resulted in a loss of compositional information resulting from temperature dependent effects. In summary, the MB parameters for the Fe3D1 and Fe3D2 doublets indicate sample-to-sample variations in mineralogical composition.

[28] With respect to the common rock-forming minerals, the MB parameters for the oct-Fe^{2+} doublets Fe2D1, Fe2D2, and Fe2D3 generally coincide with literature values for olivine ($(Fe,Mg)SiO_4$), pyroxene ($(Fe,Mg,Ca)SiO_3$), and ilmenite ($FeTiO_3$), respectively, as the Fe-bearing phases, and we (consistent with *Morris et al.* [2004]) make these assignments. Olivine and pyroxene assignments are consistent with Mini-TES spectra of Adirondack Class rock and Laguna Class soil [*Christensen et al.*, 2004]. From APXS chemistry, Adirondack Class rocks are olivine normative ($\sim Fo_{50-60}$) [*McSween et al.*, 2004, 2006]. Ilmenite was detected in rocks (Wishstone Class) that have the highest Ti concentration ($\sim$2 wt.% Ti [*Gellert et al.*, 2006; *Ming et al.*, 2006]). Therefore there is a general consensus among MER instruments for the presence of olivine, pyroxene, and ilmenite.

[29] The oct-Fe^{2+} doublet we assign to olivine (Fe2D1) has been alternatively assigned to hydrous ferrous sulfate by *Lane et al.* [2004]. However, if we assume the sulfate has a molar Fe/S ratio of $\sim$1.0 (as in simple ferrous sulfates ($FeSO_4 \bullet nH_2O$)), the ratio $[(A_{Fe2D1}Fe_T)/100]/S$ for the interiors of Adirondack Class rocks is too high ($\sim$5) to support this interpretation (elemental concentrations from *Gellert et al.* [2006]). (Parameters having the form $[(A_{FeXYZ}Fe_T)/100]$ are the product of the MB area for the FeXYZ subspectrum expressed as a fraction ($A_{FeXYZ}/100$) and the total Fe concentration (Fe_T) in units of moles of Fe per 24 moles of (O + Cl); it is the concentration of Fe from the FeXYZ phase in the target.) The ratio in Laguna Class soils is lower ($\sim$1.2), but the concentration of Fe in the Fe2D1 phase ($A_{Fe2D1}Fe_T)/100$ negatively correlates with the concentration of S, implying Fe2D1 is not a Fe^{2+} sulfate [*Yen et al.*, 2005]. In addition, the MB parameters for Fe2D1 in rock and soil are the same (Figures 4d, 5e, and 5f and Table 1), implying the same phase (olivine) in both rock and soil.

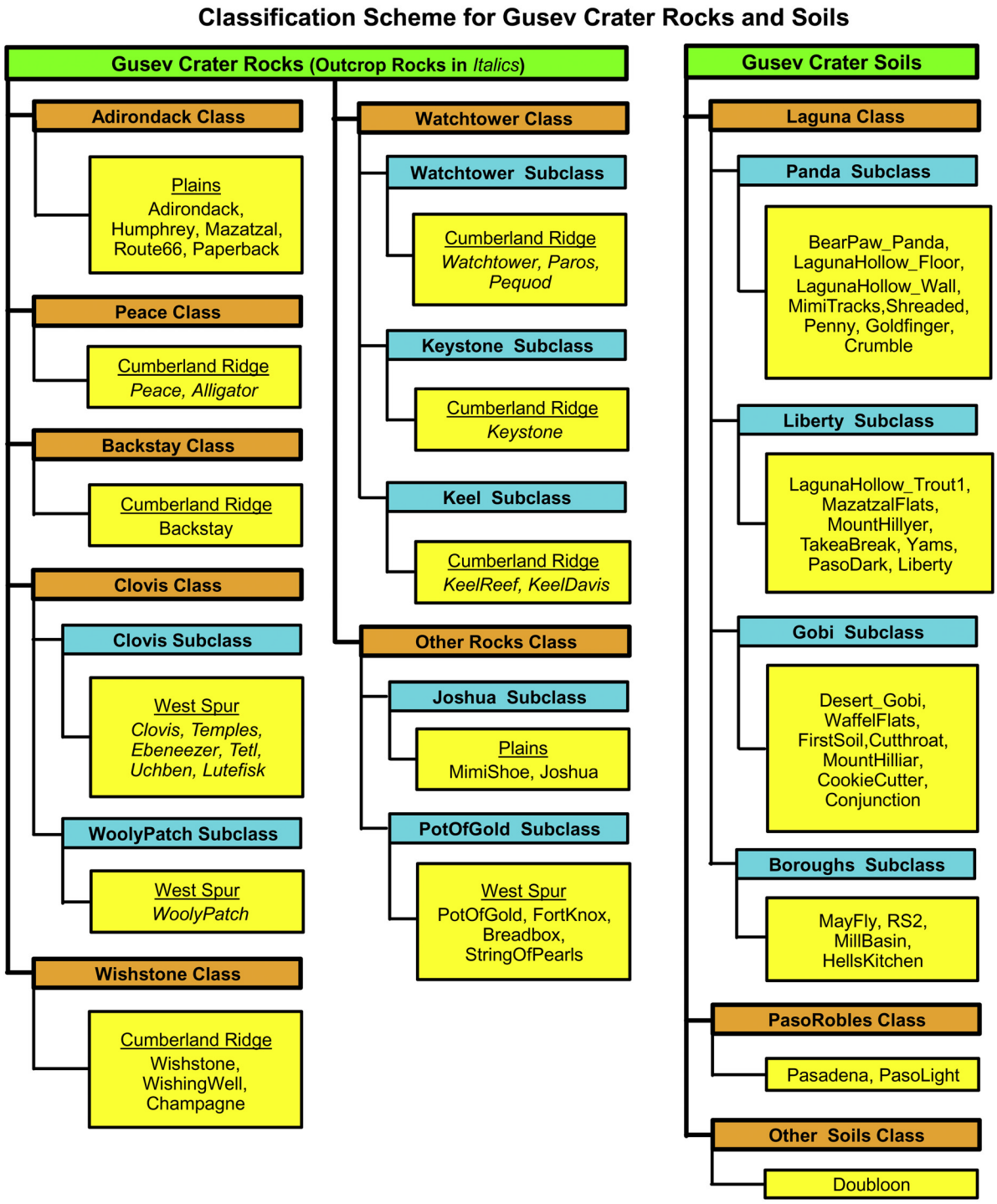

Figure 1. Classification scheme for Gusev crater rocks and soils through sol 510 of Spirit's mission. Classes for rocks [after *Squyres et al.*, 2006] and soils were formed on the basis of elemental composition, and subclasses were formed on the basis of mineralogical composition. Location names are underlined, and outcrop rocks are in italics.

[30] Because of refinements to the velocity calibration, the temperature dependence of ΔE_Q for the Fe2D1 (olivine) doublet is less than reported by *Morris et al.* [2004]. A linear least squares fit of the data in Figure 5f gives a gradient of $-(0.97 \pm 0.50) \times 10^{-4}$ mm/s/K and, by extrapolation, a quadrupole splitting of ~2.94 ± 0.04 mm/s at room temperature. This value, which remains almost exactly the value previously reported (2.92 mm/s), is the same within error of the average value of ΔE_Q for the data in Figure 5f (2.99 ± 0.04 mm/s). The average value of ΔE_Q

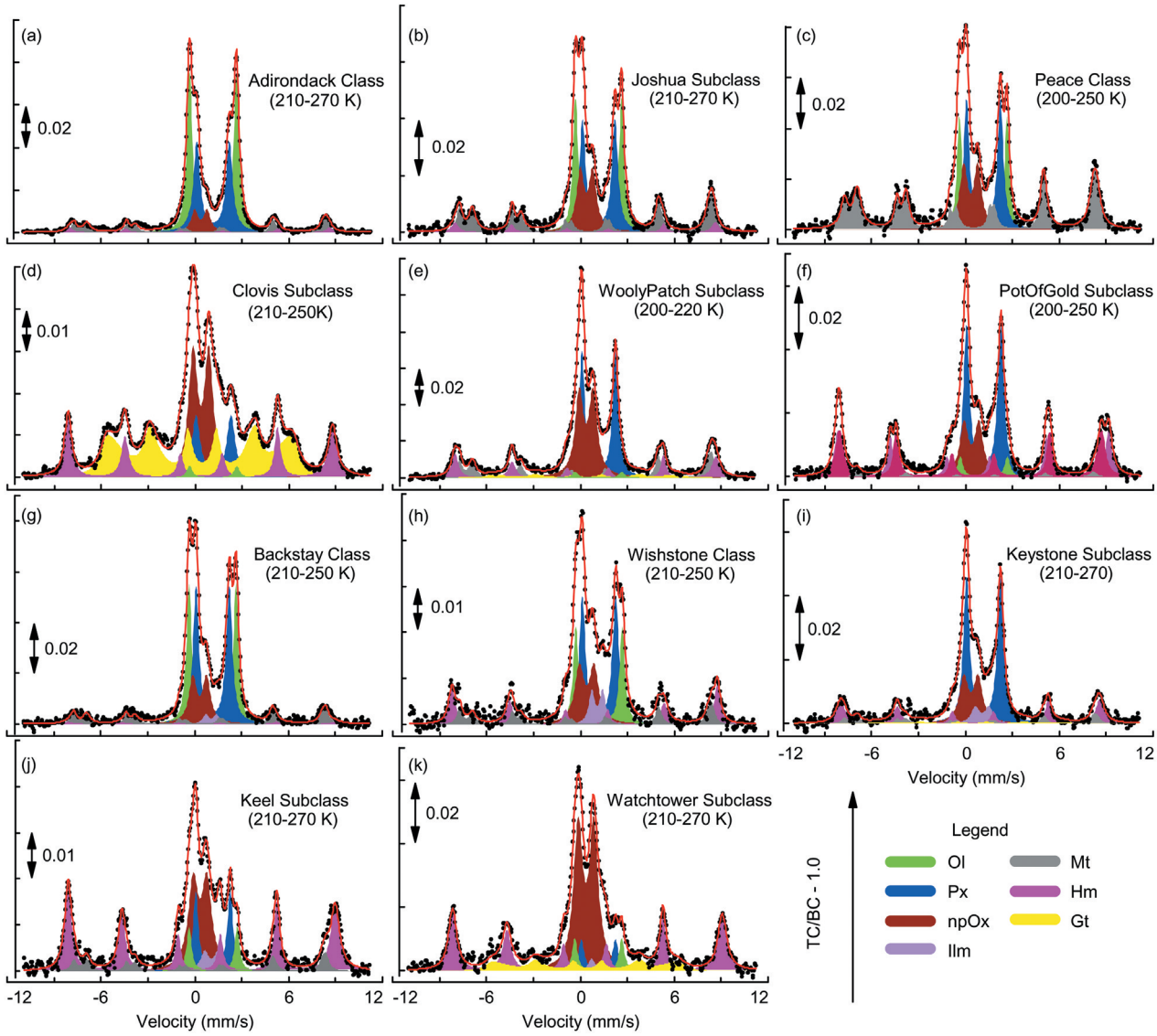

Figure 2. Representative Mössbauer spectra and subspectra obtained by least squares analysis for Gusev crater rocks. The *y* axis is the ratio of total counts to baseline counts minus one (TC/BC − 1.0). Spectra are summed over the indicated temperature range. Zero velocity is referenced with respect to metallic Fe foil at the same temperature as the Martian surface target. (a) Adirondack Class. Spectrum from sum (210–270 K) of brushed and interior surfaces of rocks Adirondack and Humphrey (A033RB0, A034RR0, A059RB0, and A060RR0). See footnote of Table 1 for explanation of sample names. (b) Joshua Subclass. Spectrum from sum (210–270 K) of undisturbed surfaces of rocks MimiShoe and Joshua (A042RU0 and A150RU0). (c) Peace Class. Spectrum (200–250 K) from interior of rock Peace (A376RR0). (d) Clovis Subclass. Spectrum (210–250 K) from sum (210–250 K) of brushed and interior surfaces of rock Clovis (A215RB0 and A218RR0). (e) WoolyPatch Subclass. Spectrum from sum (200–220 K) of interior surfaces (A198RR0 and A200RR0). (f) PotOfGold Subclass. Spectrum from sum (200–250 K) of undisturbed and interior surfaces of rock PotOfGold (A161RU0, A164RU0, A171RR0, and A173RR0). (g) Backstay Class. Spectrum (210–250 K) from brushed surface of rock Backstay (A510RB0). (h) Wishstone Class. Spectrum (210–250 K) from interior surface (A336RR0). (i) Keystone Subclass. Spectrum (210–270 K) from brushed surface of rock Keystone (A472RB0). (j) Keel Subclass. Spectrum from sum (210–70 K) of undisturbed and brushed surfaces of rocks Keel_Reef and Keel_Davis (A483RU0 and A486RB0). (k) Watchtower Subclass. Spectrum (210–270 K) from interior surface of rock Watchtower (A418RR0K).

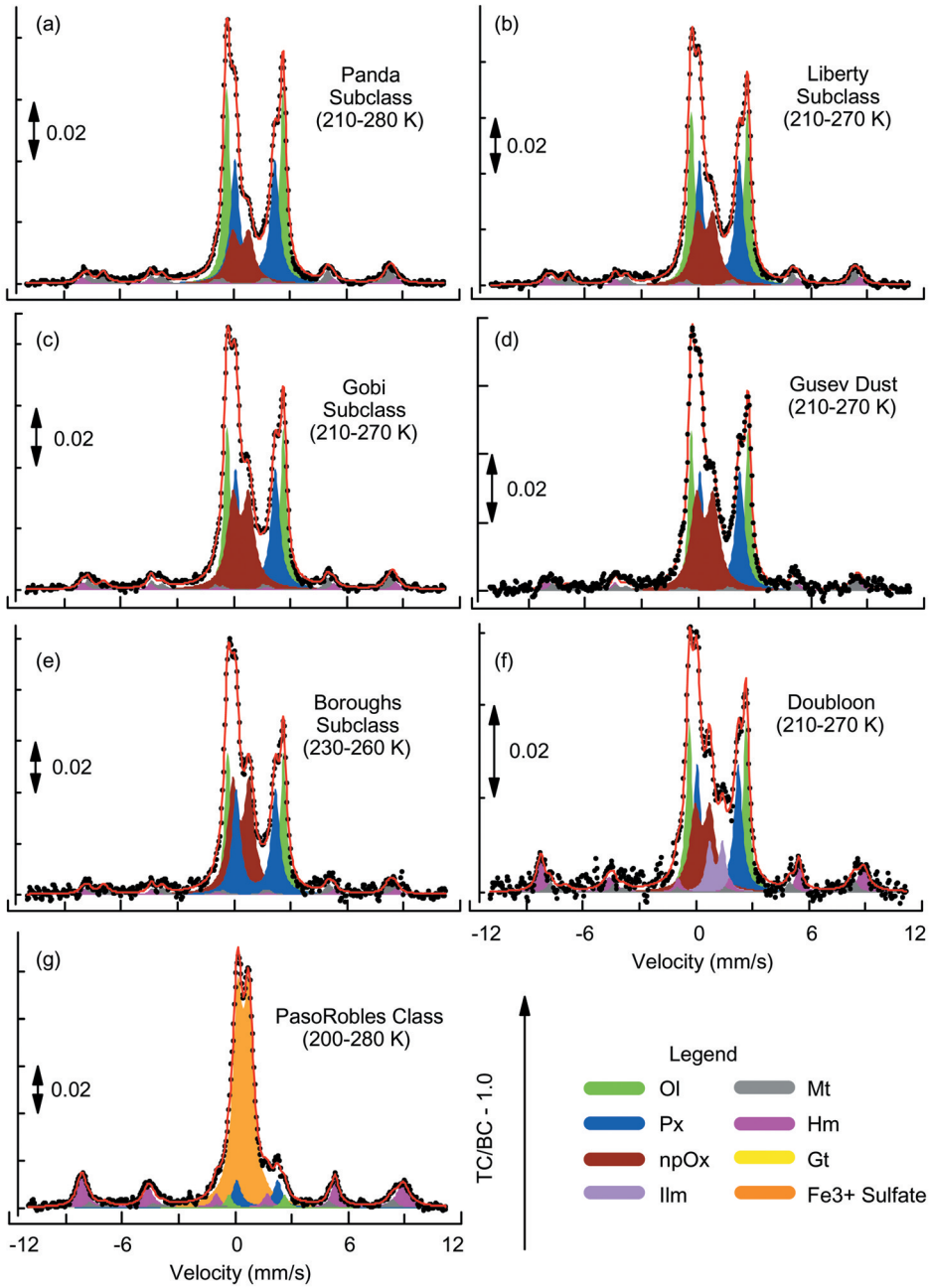

Figure 3. Representative Mössbauer spectra and subspectra obtained by least squares analysis for Gusev crater soils. Zero velocity is referenced with respect to metallic Fe foil at the same temperature as the Martian surface target. (a) Panda Subclass. Spectrum from sum (210–280 K) of disturbed and undisturbed basaltic surface soils and trench soils having relatively low contributions from npOx (A043SD0, A049ST2, A050ST1, A073SD0, A158SD0, A167SU0, A342SD0, and A459SU0). (b) Liberty Subclass. Spectrum from sum (210–280 K) of disturbed and undisturbed basaltic surface soils having intermediate contributions from npOx (A047SU0, A077SU0, A135SD0, A182SU0, A281SD0, A316SD0, A426SD0, and A479SU0). (c) Gobi Subclass. Spectrum from sum (210–270 K) of basaltic disturbed and undisturbed surface soils having high contributions from npOx (A069SU0, A110SU0, A014SU0, A122SD0, A135SD0, A182SU0, and A260SD0). (d) Spectrum of basaltic Gusev Dust as represented by the sum spectrum (210–270 K) of Desert_Gobi (A069SU0). (e) Boroughs Subclass. Spectrum from sum (230–260 K) of subsurface soils from BigHole and The Boroughs trenches (A113ST1, A114ST2, A140ST1, and A141ST2). (f) Doubloon soil. Spectrum of the only soil (210–270 K) with an ilmenite subspectrum (A502SU0). (g) PasoRobles Class. Spectrum from sum (200–280 K) of evaporite-rich disturbed soils that have high concentrations of S (A401SD0 and A429SD0).

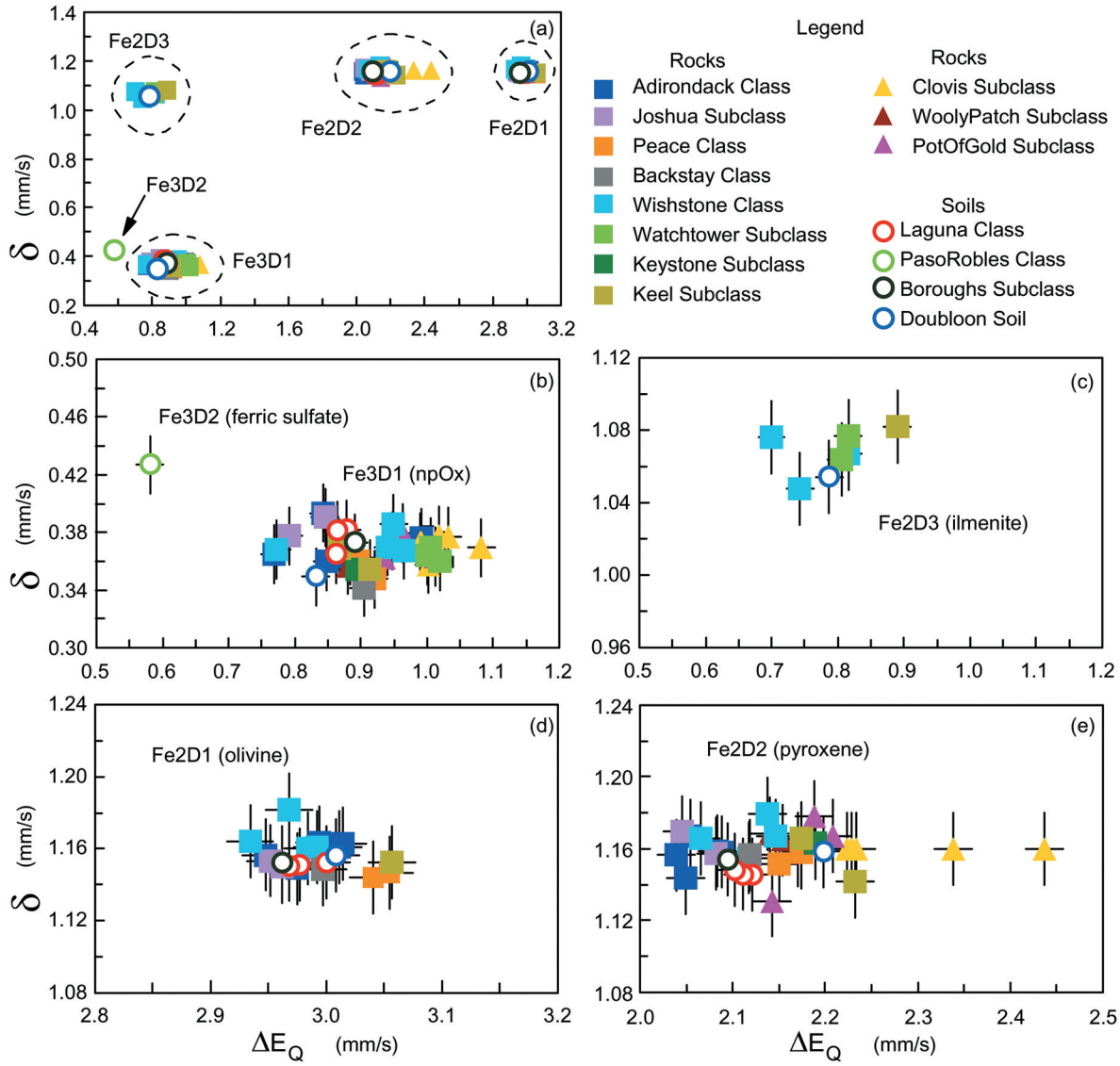

Figure 4. Isomer shift (δ) versus quadrupole splitting (ΔE_Q) for doublet subspectra. δ is referenced with respect to metallic iron foil at the same temperature as the Martian surface target. (a) Five clusters of doublet spectra are observed, three from oct-Fe^{2+} (Fe2D1, Fe2D2, and Fe2D3) and two from oct-Fe^{3+} (Fe3D1 and Fe3D2). The clusters correspond to five Fe-bearing phases. (b) Expanded scale of Figure 4a in the region of the Fe3D1 and Fe3D2 doublets which are assigned to oct-Fe^{3+} in the oxidative alteration product nanophase ferric oxide (npOx) and a Fe^{3+}-bearing sulfate, respectively. (c) Expanded scale of Figure 4a in the region of the Fe2D3 doublet which is assigned to oct-Fe^{2+} in ilmenite. (d) Expanded scale of Figure 4a in the region of the Fe2D1 doublet which is assigned to oct-Fe^{2+} in olivine. (e) Expanded scale of Figure 4a in the region of the Fe2D2 doublet which is assigned to oct-Fe^{2+} in pyroxene. The relatively large variation in ΔE_Q implies variability in Px mineralogical composition. Error bars (2σ) are given as vertical and horizontal lines extending from the individual symbols.

calculated for individual targets from spectra summed over wide temperature intervals (Table 1) is also the same within error (2.99 ± 0.06 mm/s).

[31] For the Fe2D2 (pyroxene) doublet, we do not have sufficient data to calculate a temperature dependence for ΔE_Q except for Adirondack Class rock and the aggregate of Panda, Liberty, and Gobi Subclasses of Laguna Class soil. A linear least squares fit (Figure 5d) gives quadrupole splittings of 2.07 ± 0.04 mm/s and 2.14 ± 0.04 mm/s at room temperature and gradients of $-(0.3 \pm 2.5) \times 10^{-4}$ mm/s/K and $(4.9 \pm 6.0) \times 10^{-4}$ mm/s/K, respectively (2σ standard deviations). Because the gradients are zero within error, the average values of ΔE_Q in Figure 5d over the temperature range 205–265 K for Adirondack Class and the aggregate of Laguna Subclasses (2.06 ± 0.03 mm/s and 2.11 ± 0.03, respectively) are the same within error as the extrapolated values at 295 K.

[32] The mineralogical assignment for the oct-Fe^{3+} doublet Fe3D1 is the most problematical. It is a major Fe-bearing phase, comprising ~5 to 70% of total Fe and ~25

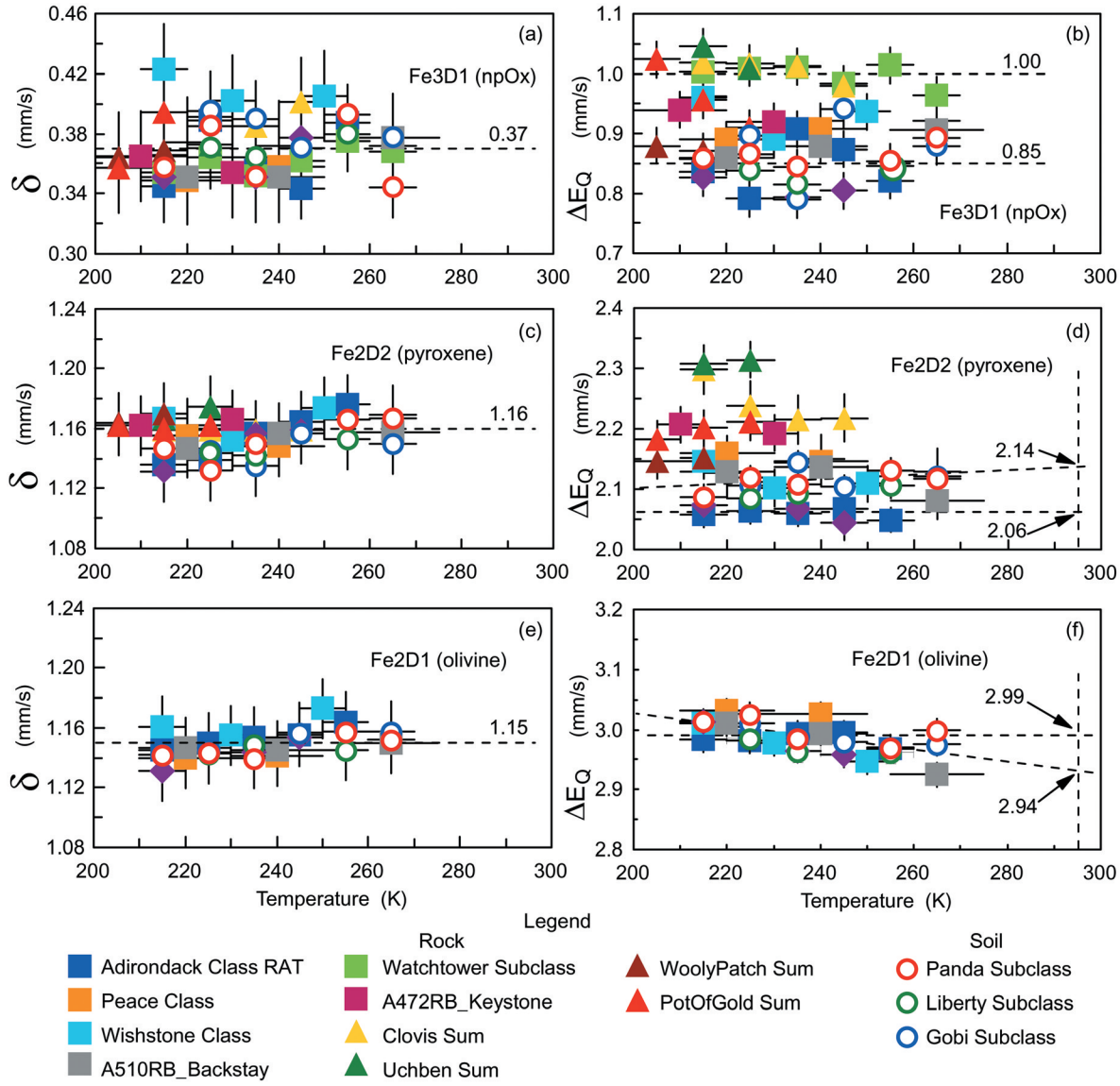

Figure 5. Isomer shift (δ) and quadrupole splitting (ΔE_Q) as a function of temperature for Fe3D1 (npOx), Fe2D2 (pyroxene), and Fe2D1 (olivine) subspectra. δ is referenced with respect to metallic iron foil at the same temperature as the Martian surface target and, within error, is not dependent on composition or temperature for (a) npOx (average = 0.37 mm/s), (c) pyroxene (average = 1.16 mm/s), and (e) olivine (average = 1.15 mm/s). ΔE_Q is dependent on composition for (b) npOx and (d) pyroxene but not, within error, for (f) olivine. A weak temperature dependence in ΔE_Q is detected for olivine. Error bars (2σ) are given as vertical and horizontal lines extending from the individual symbols.

to 100% of total Fe^{3+} (Figures 6a and 6b). A number of Fe^{3+}-bearing oxides, silicates, and sulfates have MB parameters in the range observed for this doublet and have geologically reasonable (and diverse) formation pathways. Possible formation pathways range from incorporation into silicate phases during crystallization (e.g., pyroxene and glass) to precipitation as Fe^{3+}-bearing weathering products during oxidative alteration of Fe^{2+}-bearing phases. Because δ and ΔE_Q for the Fe3D1 doublet are not mineralogically specific, we must use other information together with the MB data to infer likely mineralogical compositions.

[33] We previously assigned Fe3D1 to the alteration product nanophase ferric oxide (npOx) because its subspectral area is highest in undisturbed surface soils on the Gusev Plains, in dust coatings on rocks, and in a coherent indurated coating on the rock Mazatzal [*Morris et al.*, 2004]. The assignment is consistent with Pancam and Mini-TES spectra of the same materials. Pancam multispectral data are characterized by a Fe^{3+} absorption edge between ~400 and 750 nm, and Mini-TES spectra are interpreted as dominated by dust [*Bell et al.*, 2004; *Christensen et al.*, 2004]. After discussing our working definition for npOx, we will provide additional evidence for the assignment.

[34] NpOx is a generic name for oct-Fe^{3+} doublets from phases that are Fe^{3+}-bearing products of oxidative weathering. NpOx on Mars could result, either singly or in combi-

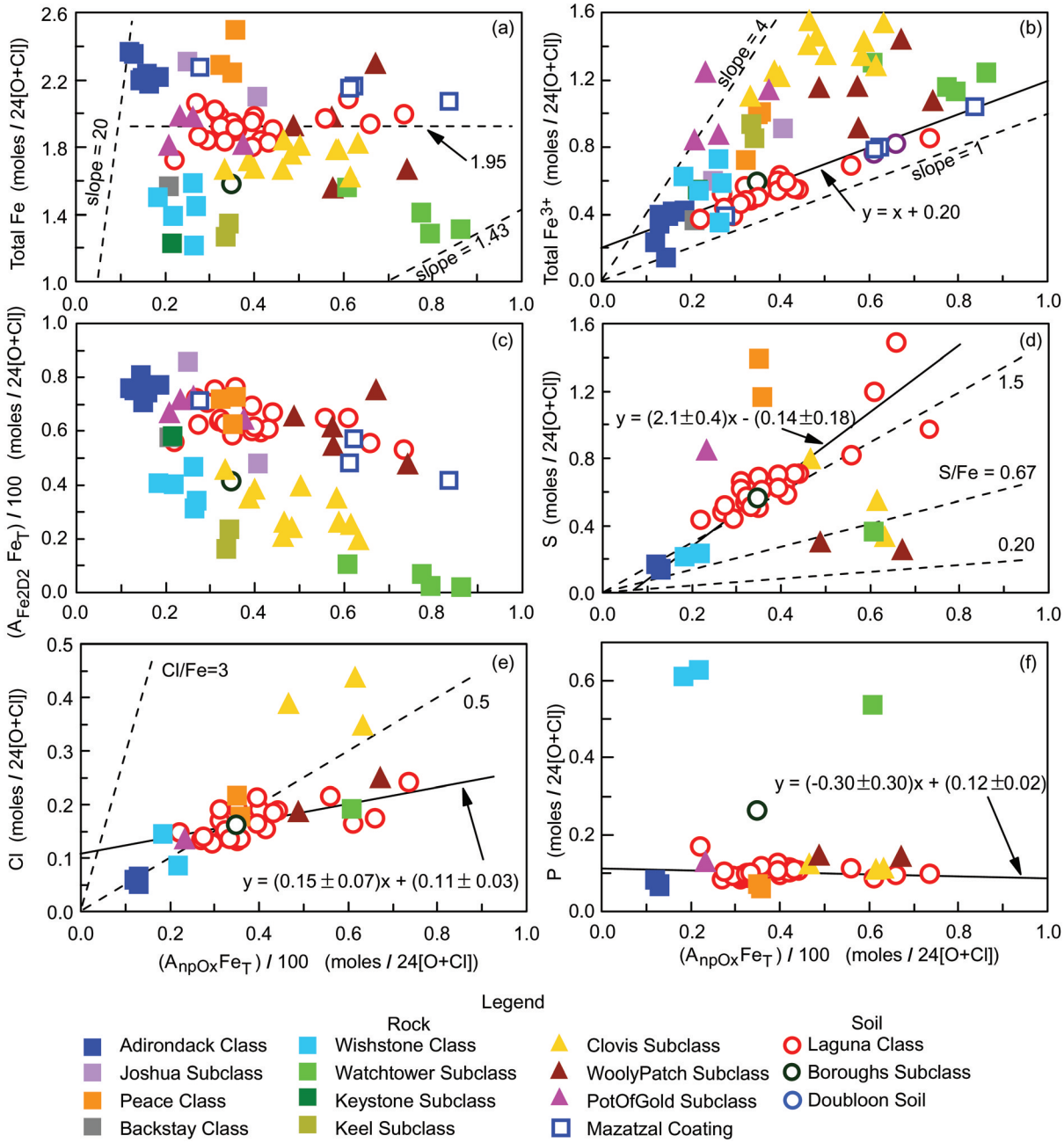

Figure 6. (a) Total iron concentration, (b) total Fe^{3+} concentration, (c) Fe concentration from the Fe2D2 (pyroxene) subspectrum, (d) S concentration, (e) Cl concentration, and (f) P concentration as a function of the concentration of Fe from npOx. Figures 6a and 6b show that npOx accounts for 5 to 70% of total iron and 25 to 100% of total Fe^{3+}, respectively, as shown by the dashed lines. The concentration of Fe from the Fe2D2 subspectrum tends to decrease as the concentration of Fe from npOx increases, showing no evidence for Fe^{3+} in Px (Figure 6c). The increases in the concentrations of S (Figure 6d) and Cl (Figure 6e) with increasing concentration of Fe from npOx imply that npOx itself is S- and Cl-bearing or formed in proportion with S- and Cl-bearing phases. The concentration of P does not vary with the concentration of Fe from npOx, implying no association of npOx with P (Figure 6f). The solid lines in Figures 6d, 6e, and 6f are least squares fits for soil data only.

nation, from a number of phases, including superparamagnetic hematite (α-Fe_2O_3) and goethite (α-FeOOH), lepidocrocite (γ-FeOOH), akaganeite (β-FeOOH), schwertmannite ($\sim Fe_8O_8(OH)_6SO_4.nH_2O$), iddingsite, ferrihydrite, and palagonite (altered basaltic glass) [*Morris et al.*, 1989, 1993, 2000, 2001, 2004; *Bishop and Murad*, 1996]. Jarosite-like phases ($(K,Na,H_3O,X^+)Fe_3(SO_4)_2(OH)_6$) can also be included in this definition, although they are more readily identified by their larger quadrupole splittings when present as well-crystalline forms. Sulfate (SO_4^{2-}) and especially phosphate (PO_4^{3-}) anions are known to undergo specific anion adsorption onto fine grained iron oxides

[e.g., *Myneni*, 2000], so that npOx can incorporate anions by this mechanism. Therefore our working definition for npOx is "a generally poorly crystalline product of oxidative weathering that contains nanometer-sized particles of Fe^{3+}-bearing material that is imbedded in a matrix and is associated with unknown proportions of H_2O, O^{2-}, OH^-, SO_4^{2-}, Cl^-, PO_4^{3-}, and other species through the formation of chemical bonds or specific chemical adsorption." Other cations can be present as substitutional impurities for Fe^{3+}. For example, Al^{3+} is a common substitutional impurity for Fe^{3+} in the terrestrial weathering environment [e.g., *Cornell and Schwertmann*, 1996].

[35] We now discuss additional evidence for the assignment of Fe3D1 to npOx. Pyroxene can accommodate Fe^{3+} in its structure to variable extents [e.g., *Rossman*, 1980]. As shown in Figure 6c, the expected negative trends (for a nonpyroxene assignment) between $A_{npOx}Fe_T/100$ and $A_{Px}Fe_T/100$ are present. We do not exclude that targets with very low values of $A_{npOx}Fe_T/100$ (e.g., the interiors of Adirondack Class rock) might have a contribution to the Fe3D1 doublet from silicate phases like pyroxene. However, we do not have observational evidence that this is the case.

[36] As discussed above, a characteristic of npOx is possible association with sulfate, chloride, and phosphate anions. In Figures 6d, 6e, and 6f, we plot the concentration of S, Cl, and P as a function of $A_{npOx}Fe_T/100$ for soils and interiors of rocks exposed by the MER Rock Abrasion Tool. The solid lines in each figure are the least squares fits for the soil data only. As discussed by *Yen et al.* [2005] for the S data, the positive correlation between $A_{npOx}Fe_T/100$ and S for soil suggests that npOx is itself a S-bearing phase, is not a S-bearing phase but is formed along with a S-bearing and Fe-free phase in approximately fixed proportions, or is a S-bearing phase and formed along with another S-bearing and Fe-free phase in approximately fixed proportions. Surprisingly, the S/Fe stoichiometry implied by the correlation is 2/1, which is even more S-rich than the 3/2 ratio for simple hydrated Fe^{3+} sulfates ($Fe_2(SO_4)_3.nH_2O$). The ratios for jarosite and schwertmannite are 2/3 and 1/5 to 1/8, respectively [*Bigham and Nordstrom*, 2000]. Although possible, we consider it unlikely that substantially all S is combined with Fe to form a simple sulfate. The excess Mg and S in Boroughs Subclass soil relative to other Laguna Class soil has been attributed to Mg sulfates, implying that Mg sulfates are reasonably present at some level in other soils because of impact and aeolian mixing [e.g., *Haskin et al.*, 2005]. Mg sulfates are also inferred to be present in Peace Class rocks as a cement [*Ming et al.*, 2006]. The Mössbauer spectra of all hydration states of simple ferric sulfates are not known to us, but the n = 7 (kornelite) and n = 9 (coquimbite) hydrates have quadrupole splittings (<0.6 mm/s) that are small relative to those for the npOx doublet (0.7–1.0 mm/s). There is evidence for a Fe^{3+}-bearing sulfate in Gusev crater, and its MB parameters are different from those for the npOx doublet (discussed below). However, this observation is a weak constraint because it only excludes that particular sulfate from making significant contributions to Laguna Class soil. And finally, there is a positive correlation of $A_{npOx}Fe_T/100$ with the concentration of Cl (Figure 6e), implying an association of npOx with both sulfate and chloride anions. A Cl/Fe stoichiometry of ~1/7 is implied if all Cl is associated with Fe in npOx. We found no correlation between $A_{npOx}Fe_T/100$ and the concentration of P (Figure 6f).

[37] The sense of Figure 6 is that Laguna Class soil is a mixture of a highly weathered, S-rich component that contains npOx as its primary Fe-bearing phases and other materials that are mechanical degradation products of rocks that have low levels of S, Cl, and P in their interiors. Because of their high P (and Ti) contents [*Ming et al.*, 2006], Wishstone and Watchtower Class rocks do not make a significant contribution to Laguna Class soil. A possible generalized chemical formula for npOx is $[Fe_{1-x}(M_mA_aB_b)_x][O_v(OH)_w(SO_4)_yCl_z(H_2O)_n]$ where M = Al^{3+}, Cr^{3+}, etc., A = Ca^{2+}, Mg^{2+}, etc., B = Na^+, K^+, etc., $x < 1$, $3m + 2a + b = 3$, $v < 1.5$, $w < 3$, $y < 1.5$, $z < 0.14$, $n \geq 0$, and $2v + 2y + w + z = 3$. We have no direct evidence that other cations substitute for Fe in MER MB spectra, but Al is a common substitutional impurity for Fe in the terrestrial weathering environment [*Cornell and Schwertmann*, 1996]. For x = 0, chemical formulas for possible end-members are Fe_2O_3 (superparamagnetic hematite) for v = 1.5 and n = 0; FeOOH (superparamagnetic goethite) for v = w = 1 and n = 0; $Fe_{10}O_6(OH)_{18}$ (ferrihydrite) for v = 0.6, w = 1.8, and n = 0; $(H_3O)Fe_3(SO_4)_2(OH)_6$ (hydronium jarosite) for w = 1.67, y = 0.67, n = 0.67; $Fe_8O_8(OH)_6SO_4 \bullet nH_2O$ (schwertmannite) for v = 1, w = 0.75, and y = 0.125; and $FeO(OH)_wCl_z$ (akaganeite) for v = 1 and w + z = 1. The high Cl and especially S concentrations on Mars increases the likelihood of akaganeite-like, schwertmannite-like, and Fe^{3+}-sulfate-bearing phases in general as alteration products relative to Earth. We tried to constrain the mineralogical, and therefore the chemical, composition of npOx through elemental correlations with quadrupole splittings. We could not find a systematic satisfactory correlation, possibly because npOx is not the dominant phase for any of the anions with which it is associated or perhaps composition is not the controlling parameter for ΔE_Q.

3.3.2. Fe2D3 and Fe3D2

[38] The Fe2D3 doublet is found only in the Columbia Hills in the Wishstone and Watchtower Class rocks and in the soil Pequod_Doubloon. Because the values of the Mössbauer parameters (Table 2 and Figure 4) are consistent with the mineral ilmenite ($FeTiO_3$) and because these rocks and soil have high concentrations of Ti relative to other Gusev rocks and soils, we assign Fe2D3 to ilmenite.

[39] The Fe3D2 doublet is found only in the Columbia Hills in the two soils of PasoRobles Class. The soils are so rich in sulfur (~3.2 moles per 24(O + Cl), which is more than twice any other Gusev sample and even more than the Meridiani Planum outcrop [*Rieder et al.*, 2004; *Gellert et al.*, 2006; *Ming et al.*, 2006]) that Fe has to be bound to sulfate by cation-anion abundance considerations if all S is present as sulfate anion. The Fe3D2 doublet is clearly distinguished from npOx by its higher δ (~0.43 mm/s) and lower ΔE_Q (~0.58 mm/s) (Table 2 and Figure 4). Both observations, taken together, imply that Fe3D2 is a Fe^{3+}-bearing sulfate.

3.4. Mineralogical Assignment of Sextet Subspectra

[40] We identified 4 sextets in Gusev crater Mössbauer spectra (Fe3S1, Fe2.5S1, Fe3S2, and Fe3S3). Figure 7 is a plot of B_{hf} as a function of ΔE_Q for these sextets (Table 3), and their values of δ are indicated in the figure. The MB

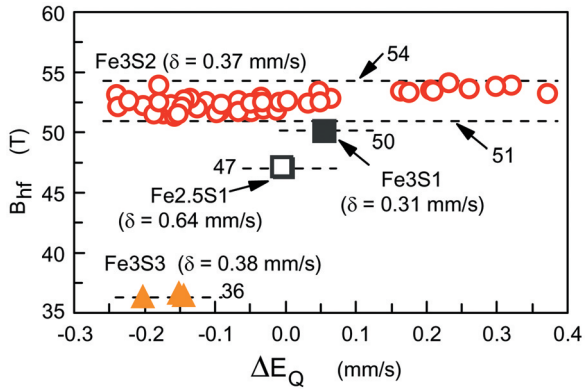

Figure 7. Hyperfine field strength (B_{hf}) versus quadrupole splitting for sextet subspectra (200–280 K). Fe3S1 and Fe2.5S1 are subspectra from tet-Fe^{3+} and oct-$Fe^{2.5+}$ in magnetite. The Fe3S2 subspectrum is from oct-Fe^{3+} in hematite, and a range of values is present because diurnal temperature variations on Mars cycle through the temperature of the Morin transition (~260 K). The Fe3S3 subspectrum is from oct-Fe^{3+} in goethite.

parameters were derived for individual targets from spectra summed over a wide temperature interval, to optimize counting statistics. Comparison of the MB parameters to literature data readily identifies the subspectra sextets as the tet-Fe^{3+} and oct-$Fe^{2.5+}$ sites of magnetite (Mt, Fe_3O_4), the oct-Fe^{3+} site of hematite (Hm, α-Fe_2O_3), and the oct-Fe^{3+} site of goethite (Gt, α-FeOOH), respectively. All these oxides are common on the Earth [e.g., *Cornell and Schwertmann*, 1996]. The cations Cr^{3+} and especially Al^{3+} are common substitutional impurities for Fe^{3+} [e.g., *Cornell and Schwertmann*, 1996]. In igneous rocks, titanomagnetites ($Ti_xFe_{3-x}O_4$) are common, and their Mössbauer spectra at low Ti concentrations are double sextet patterns like magnetite [e.g., *Tanaka and Kono*, 1987; *Morris et al.*, 1993]. In stoichiometric magnetite, the ratio of Fe atoms on the octahedral to tetrahedral sites is 2, so that the ratio of the corresponding subspectral areas is ~2. Substitutional impurities and/or deficiency in the Fe^{2+} cation results in deviations from the ratio, normally to lower values [e.g., *Daniels and Rosencwaig*, 1969; *Morris et al.*, 1985; *Murad and Johnston*, 1987; *Ramdani et al.*, 1987].

[41] The range in values of B_{hf} and ΔE_Q for hematite results because the oxide undergoes a magnetic transition (the Morin transition) where those parameters change values at temperatures realized by the Martian diurnal cycle. The Morin transition temperature (T_M) occurs near 260 K for chemically pure, well-crystallized, bulk hematite. Substitutional impurities like Al^{3+} lower the transition temperature and broaden the temperature interval over which it occurs [e.g., *Murad and Johnston*, 1987; *De Grave and Vandenberghe*, 1990; *Dang et al.*, 1998]. For MB parameters, ΔE_Q is <0 for $T > T_M$, $\Delta E_Q > 0$ for $T < T_M$, and B_{hf} for $T < T_M$ is larger than B_{hf} for $T > T_M$. This relationship is present in Figure 7, providing additional evidence for the hematite assignment.

[42] Representative laboratory transmission MB spectra (298 K) of well-crystalline Mt, Hm, Gt, and maghemite (Mh, γ-Fe_2O_3) are shown in Figure 8a [after *Morris et al.*, 1985, 2000]. The transmission spectra are inverted for easier comparison to Martian spectra. The Mh spectrum resembles and can be fit by a single sextet, but it is actually a double sextet pattern (one site each oct-Fe^{3+} and tet-Fe^{3+}) where the two sites are nearly equivalent. As shown by the dashed vertical lines, which are located at the center positions of the Mt tet-Fe^{3+} peaks, the peak positions for the Mt tet-Fe^{3+} and the maghemite sextets are nearly the same. Thus we are not able to uniquely assign the Fe3S1 subspectrum to either magnetite or maghemite on the basis of its MB parameters alone. However, the presence of an oct-$Fe^{2.5+}$ sextet (Fe2.5S1) implies the Fe3S1 sextet is at least in part the second magnetite sextet. The absence of the oct-$Fe^{2.5+}$ sextet implies the Fe3S1 sextet is maghemite. Usually, the oct-$Fe^{2.5+}$ sextet is present in Gusev spectra along with the tet-Fe^{3+} sextet, so that we assign both sextets to magnetite or nonstoichiometric magnetite if $A_{Mt(oct)}/A_{Mt(tet)}$ is not ~2. Representative subspectra for Gt, Hm, and Mt from least squares fits of Martian spectra are shown in Figure 8b. The subspectrum for Mt in Peace has approximately the stoichiometric ratio ($A_{Mt(oct)}/A_{Mt(tet)} = 1.6 \pm 0.4$). We previously reported a ratio of ~1 for Gusev Plains targets, implying nonstoichiometric magnetite (ns-magnetite) [*Morris et al.*, 2004]. The PotOfGold spectra are noteworthy, because they have two Hm subspectra (one from Hm above and one from Hm below the Morin transition).

3.5. Summary

[43] Through sol 510 at Gusev crater, the Mössbauer spectrometer on the MER Spirit rover has identified 8 Fe-bearing phases. Two are Fe^{2+} silicates (olivine and pyroxene), one is a Fe^{2+} oxide (ilmenite), one is a mixed Fe^{2+} and Fe^{3+} oxide (magnetite), two are Fe^{3+} oxides (hematite and goethite), one is a Fe^{3+} sulfate (mineralogically not constrained), and one is a complex Fe^{3+} phase (npOx). We envision that npOx is poorly crystalline (short-range order or amorphous) without distinct mineralogical composition and with a diffuse chemical composition that depends on local conditions. Element correlations indicate npOx has an association with sulfate and chloride anion either through the formation of chemical bonds, specific chemical adsorption, or as individual precipitates that have formed via alteration processes. The behavior of hematite is complex because the temperature of the Morin transition (~260 K) lies within diurnal temperature variations on Mars. Goethite is the only unequivocal H_2O/OH bearing phase, and it yields ~10% H_2O upon dehydroxylation. As an alteration product, npOx also likely contains H_2O/OH, but the evidence is inferential. A hydrous Fe^{3+}-sulfate is inferred from combined MB, APXS, Mini-TES, and Pancam data.

[44] We next discuss the Mössbauer mineralogy of rocks and soils at Gusev crater as revealed by Spirit on its journey through the Gusev Plains and into the Columbia Hills during the first 510 sols.

4. Mössbauer Mineralogy of Gusev Crater

4.1. Fe Oxidation State

[45] The distribution of Fe among its oxidation states is a key parameter for understanding the prevailing redox conditions during crystallization of minerals from lava and

during weathering and alteration. In Figures 9a and 9b we plot the total Fe concentration (Fe_T) [*Gellert et al.*, 2006] and the Fe^{3+}/Fe_T ratio as a function of sol number (a proxy for location). For rocks, Fe_T varies by about a factor of 2, and, except for Peace Class rocks, there is a general decrease in Fe_T as Spirit traversed eastward from the Gusev plains into the West Spur and Husband Hill regions of the Columbia Hills. Except for the soil Pasadena_PasoRobles, Fe_T for soils is more nearly constant (average $\pm 2\sigma = 1.9 \pm 0.2$ moles/24(O + Cl)), although there is a slight trend to lower Fe_T concentrations from west to east.

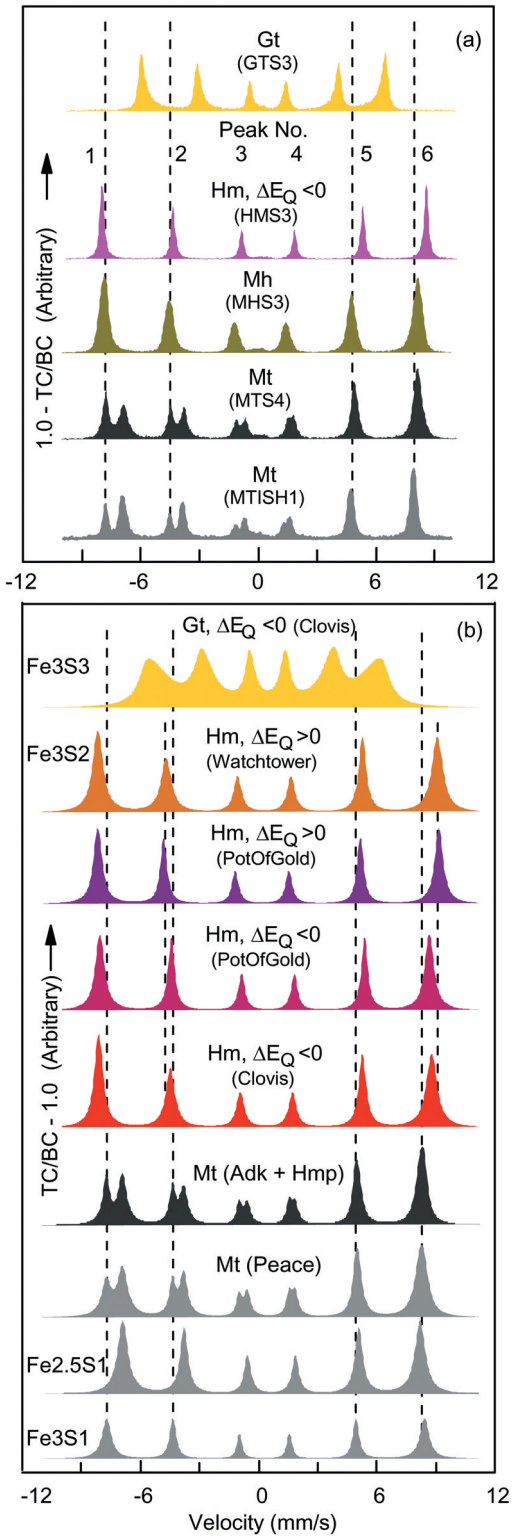

[46] The difference in Fe^{3+}/Fe_T for rocks in the plains and rocks in the Columbia Hills is dramatic. Adirondack Class rocks, the dominant rock type on the plains, are characterized by relatively low values of Fe^{3+}/Fe_T (average $\pm 2\sigma = 0.12 \pm 0.10$). For West Spur and Husband Hill, there are a number of outcrop rocks with very high Fe^{3+}/Fe_T ratios. The values (average $\pm 2\sigma$) for Clovis and Watchtower Class rocks (total of 13 rocks (Table 6)) are 0.72 ± 0.18 and 0.74 ± 0.36, respectively. The most oxidized rocks are Clovis and Paros with $Fe^{3+}/Fe_T = 0.84$ and 0.94, respectively. Furthermore, the oxidation is pervasive and not just a thin surface alteration zone because interior rock exposed by the RAT has comparable (WoolyPatch and Clovis) to somewhat higher (Ebenezer and Uchben) values of Fe^{3+}/Fe_T (Table 5) than rock surfaces. This situation is unlike the Adirondack Class rock Mazatzal which has a thin rind or coating that is oxidized relative to interior rock [*Haskin et al.*, 2005]. The exterior (A080RB0 Mazatzal_NewYork) and interior (A084RR0 Mazatzal_Brooklyn) surfaces, revealed by brushing and then grinding with the RAT, have $Fe^{3+}/Fe_T = 0.36$ and 0.10, respectively (Table 5).

[47] The values of Fe^{3+}/Fe_T for Laguna Class soils (all but 3 soils are in this class) are relatively constant (average $\pm 2\sigma = 0.30 \pm 0.14$). PasoRobles Class soil is very oxidized ($Fe^{3+}/Fe_T \sim 0.83$).

[48] Because all npOx, Hm, and Gt are products of weathering and alteration, the sum $A_{npOx} + A_{Hm} + A_{Gt} + A_{Sulfate}$ can be used as a mineralogical alteration index (MAI). Likewise, the sum $A_{Ol} + A_{Px} + A_{Ilm} + A_{Mt}$ can be used as an index in the opposite sense, assuming that magnetite is a primary phase. The two indices are plotted against each other in Figure 9c. The Adirondack, Backstay, and Peace Class rocks are the least altered with MAI < 20%. The most altered rocks are Clovis and Watchtower Subclass with MAI > 80%.

4.2. Mössbauer Mineralogy of Rocks

[49] An overview of the type and distribution of Gusev crater rocks is given by *Arvidson et al.* [2006]. *Squyres et al.*

Figure 8. (a) Inverted laboratory transmission spectra (295 K) for well-crystalline goethite (Gt), hematite (Hm), maghemite (Mh), and two magnetite (Mt) samples with different ratios for their tet-Fe^{3+} and oct-$Fe^{2.5+}$ subspectra. Dashed vertical lines go through the center positions for peaks 1, 2, 5, and 6 of the tet-Fe^{3+} sextet of Mt. The peak centers for Mh occur at nearly the same positions, so that the $Fe^{2.5+}$ magnetite subspectrum must be present to assign both subspectra to magnetite (or nonstoichiometric magnetite). (b) Gt, Hm, and Mt subspectra abstracted from least squares fits of several Martian surface targets (210–280 K). Sextet peak areas were constrained to 3:2:1:1:2:3 during the fitting procedure. Dashed vertical lines are drawn through the center positions of peaks 1, 2, 5, and 6 of the tet-Fe^{3+} subspectrum. The PotOfGold target has two hematite subspectra, corresponding to the presence of hematite both above and below the Morin transition temperature. Sextet peak areas were constrained to 3:2:1:1:2:3 during the fitting procedure.

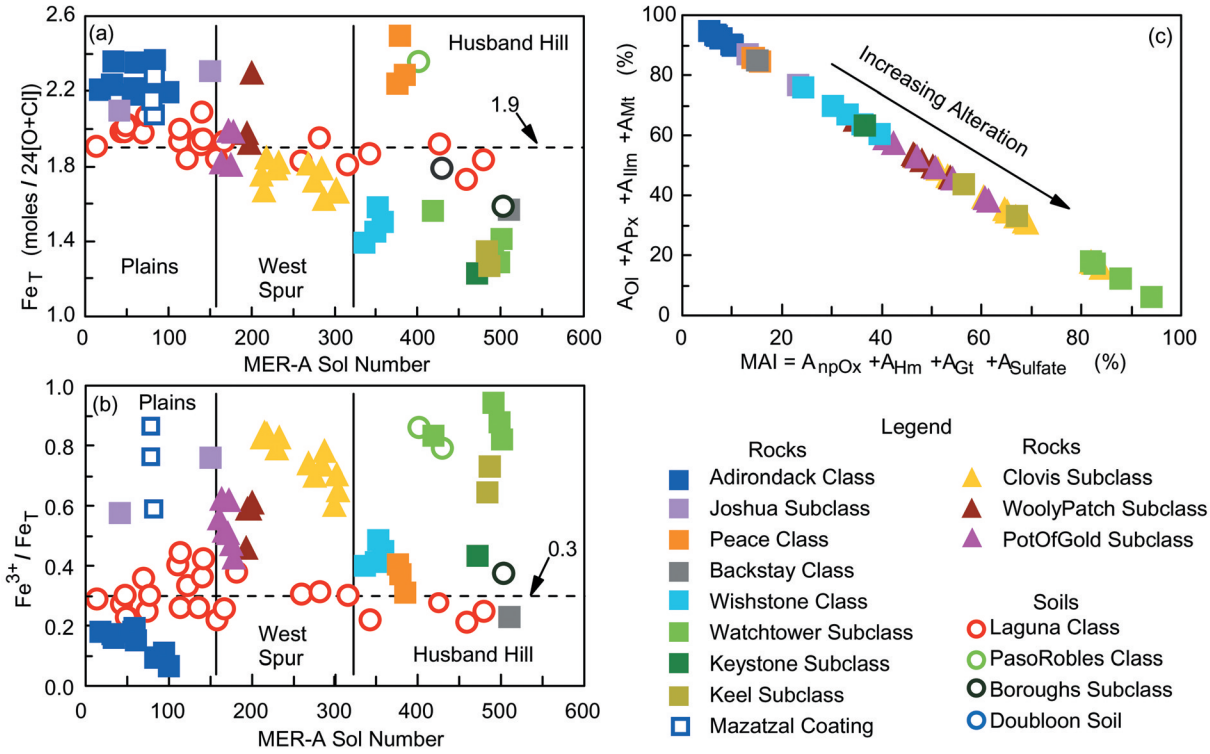

Figure 9. (a) Total Fe concentration (Fe_T) and (b) Fe^{3+}/Fe_T ratio as a function of sol number for Spirit's mission. Except for Peace Class, Fe_T for rocks generally decreased as Spirit roved from the plains into the Columbia Hills. The oxidation state of rocks is highly variable, with the plains having mostly relatively unaltered Adirondack Class rocks and the Columbia Hills having pervasively altered rocks (Clovis, Wishstone, and Watchtower Classes). The basaltic soils (Laguna Class) have relatively constant Fe concentration and oxidation state. The two evaporite-rich soils of PasoRobles Class are very oxidized relative to Laguna Class soil. (c) $A_{Ol} + A_{Px} + A_{Ilm} + A_{Mt}$ versus $A_{npOx} + A_{Hm} + A_{Gt} + A_{Sulfate}$. The wide range in the state of alteration is shown by the mineralogical alteration index (MAI = $A_{npOx} + A_{Hm} + A_{Gt} + A_{Sulfate}$).

[2006] provide a synthesis of chemical, mineralogical, and textural properties of Columbia Hills rocks that is organized around five major rock classes (Backstay, Peace, Wishstone, Clovis, and Watchtower). In this section, we discuss the mineralogical composition of these classes plus Adirondack Class from the perspective of Fe-bearing phases according to Mössbauer spectroscopy (Mössbauer mineralogy). Because some of the classes are composed of rocks having distinctly different mineralogical compositions, we further subdivided some classes into subclasses (Figure 1). This included forming subclasses for the rocks in the Other Rocks Class. Pie diagrams showing the distribution of Fe among Fe-bearing phases in the classes and subclasses are given in Figure 10 (data from Table 6). The percentages given in the figure for Ol, Px, Mt, etc. are the relative proportions of Fe from (or associated with) those phases and not the actual modal or weight percentage of Ol, Px, etc. in the bulk rock. General geographical locations of rocks are shown in Figure 9.

4.2.1. Adirondack Class, Backstay Class, Peace Class, and Joshua Subclass

[50] Adirondack Class rocks are the dominant rock type on the Gusev Plains. Adirondack, Humphrey, Mazatzal, and Route66 were studied in detail, and they are the least altered rocks encountered by Sprit as of sol 510 (class average MAI = 7%). MB analysis shows that 51% of total Fe is from Ol, 34% from Px, 8% from Mt, 6% from npOx, and minor Fe from Hm. Backstay Class rock (only Backstay analyzed by APXS and MB) is slightly more altered (MAI = 15%), although this value may be anomalously high because we only have analyses of the exterior, possibly weathered, surface. The rock has ~36% Fe from each of Ol and Px, 13% from npOx, 10% from Mt, and minor Fe from Hm and Ilm. Peace Class (Peace and Alligator) is altered to the same extent as Backstay Class, and average Peace Class has ~28% Fe from each of Ol, Px, and Mt and 15% Fe from npOx. Peace Class rock has the highest Fe from Mt of any rock analyzed at Gusev crater as of sol 510. Peace and Backstay Class rocks are located on Husband Hill (Figure 9).

[51] The Joshua Subclass includes two float rocks from the plains (MimiShoe and Joshua). The subclass average has MAI = 18% and 30% of Fe from each of Ol and Px, 22% from Mt, 15% from npOx, and 3% from hematite.

[52] The ratio of Fe from Ol to Fe from Px (A_{Ol}/A_{Px}) for Backstay Class, Peace Class, Joshua Subclass, and also Wishstone Class rocks is ~1.0. The ratio for Adirondack Class rocks is substantially different (~1.5). As discussed below, this difference limits the contribution of mechanical degradations products of Adirondack Class rocks to Gusev soil.

[53] The presence of Mt in these four relatively unaltered groups of rocks is consistent with crystallization from lava

Table 6. Average Mössbauer Areas for Component Subspectra (f-Factor Corrected) and Fe^{3+}/Fe_T for Individual Rocks and for Classes and Subclasses of Gusev Crater Rocks

Generic Name Assignment	Fe2D1 Ol, %	Fe2D2 Px, %	Fe2D3 Ilm, %	Fe3D1 npOx, %	Fe3D2 Sulfate, %	Mt, %	Fe3S1 Mt(tet), %	Fe2.5S1 Mt(oct), %	Fe3S2 Hm, %	Fe3S3 Gt, %	Total, %	Fe^{3+}/Fe_T
Adirondack Class												
Adirondack	47	33	0	6	0	13	5	8	1	0	100	0.17
Humphrey	47	34	0	7	0	11	6	5	2	0	100	0.17
PaperBack	41	36	0	19	0	3	3	1	0	0	100	0.23
Mazatzal	57	32	0	5	0	6	3	3	0	0	100	0.10
Route66	57	37	0	7	0	0	0	0	0	0	100	0.07
Average	52	34	0	6	0	8	3	4	1	0	100	0.12
1σ Std. Dev.[a]	6	2	2	2	2	6	3	3	2	2		0.05
Clovis Class												
Average	2	23	0	29	0	15	7	8	13	19	100	0.72
1σ Std. Dev.[a]	2	8	2	7	2	7	3	4	4	11		0.09
Clovis Class, Clovis Subclass												
Clovis	2	14	0	27	0	1	1	1	19	37	100	0.84
Ebenezer	1	13	0	34	0	20	9	11	14	20	100	0.81
Temples	1	22	0	28	0	10	5	5	13	26	100	0.74
Tetl	2	21	0	23	0	24	10	14	16	15	100	0.70
Uchben	2	18	0	35	0	13	6	8	8	23	100	0.76
Lutefisk	2	25	0	22	0	17	7	10	15	19	100	0.68
Average	2	19	0	28	0	14	6	8	14	23	100	0.76
1σ Std. Dev.[a]	2	5	2	6	2	8	3	5	4	8		0.06
Clovis Class, WoolyPatch Subclass												
WoolyPatch	3	37	0	25	0	15	8	7	14	6	100	0.56
1σ Std. Dev.[b]	2	8	0	5	0	2	2	4	4	2		0.07
Wishstone Class												
Wishstone	20	29	8	16	0	12	7	5	14	0	100	0.40
WishingWell	29	24	3	19	0	10	6	5	14	0	100	0.41
Champagne	18	28	6	14	0	10	8	2	9	15	100	0.47
Average	23	27	6	16	0	11	7	4	13	5	100	0.43
1σ Std. Dev.[a]	6	3	2	2	2	2	2	2	3	9		0.04
Peace Class												
Peace	22	29	0	15	0	34	13	21	0	0	100	0.39
Alligator	32	31	0	14	0	23	11	12	0	0	100	0.31
Average	27	30	0	15	0	28	12	16	0	0	100	0.35
1σ Std. Dev.[a]	7	2	2	2	2	8	2	6	2	2		0.06
Watchtower Class												
Average	6	15	4	39	0	5	2	3	25	6	100	0.74
1σ Std. Dev.[a]	5	17	3	19	2	5	3	3	10	6		0.18
Watchtower Class, Watchtower Subclass												
Watchtower	7	7	3	39	0	1	0	1	31	12	100	0.83
Paros	3	1	2	66	0	0	0	0	18	11	100	0.94
Pequod	5	3	6	58	0	0	0	0	16	11	100	0.85
Average	5	4	4	54	0	0	0	0	22	11	100	0.87
1σ Std. Dev.[a]	2	3	2	14	2	2	2	2	8	2		0.06
Watchtower Class, Keystone Subclass												
Keystone	0	47	6	17	0	10	4	6	15	4	100	0.43
1σ Std. Dev.[c]	2	2	2	2	2	2	2	2	2	2		0.03
Watchtower Class, Keel Subclass												
KeelReef	15	18	1	25	0	10	6	4	31	0	100	0.64
KeelDavis	4	13	8	27	0	9	3	5	40	0	100	0.73
Average	9	15	4	26	0	9	5	5	36	0	100	0.69
1σ Std. Dev.[a]	8	3	5	2	2	2	2	2	7	2		0.06
Backstay Class												
Backstay	35	37	3	13	0	11	5	6	2	0	100	0.23
1σ Std. Dev.[c]	2	2	2	2	2	2	2	2	2	2		0.03
Other Plains Rocks, Joshua Subclass												
MimiShoe	28	23	0	19	0	26	13	14	4	0	100	0.43
Joshua	33	37	0	11	0	17	8	9	2	0	100	0.26
Average	30	30	0	15	0	22	10	11	3	0	100	0.34
1σ Std. Dev.[a]	4	10	2	6	2	7	3	4	2	2		0.12

Table 6. (continued)

Generic Name Assignment	Fe2D1 Ol, %	Fe2D2 Px, %	Fe2D3 Ilm, %	Fe3D1 npOx, %	Fe3D2 Sulfate, %	Mt, %	Fe3S1 Mt(tet), %	Fe2.5S1 Mt(oct), %	Fe3S2 Hm, %	Fe3S3 Gt, %	Total, %	Fe^{3+}/Fe_T
Other West Spur Rocks, PotOfGold Subclass												
PotOfGold	5	36	0	16	0	3	1	2	40	0	100	0.58
FortKnox	10	37	0	13	0	2	0	2	38	0	100	0.52
BreadBox	14	37	0	11	0	6	4	2	31	0	100	0.47
StringOfPearls	19	37	0	13	0	4	0	3	27	0	100	0.43
Average	12	37	0	13	0	4	1	3	34	0	100	0.50
1σ Std. Dev.[a]	6	2	2	2	2	2	2	2	6	2		0.06

[a]Standard deviation of class members or 2%, whichever is larger, for subspectral areas.
[b]Standard deviation of multiple measurements on the same rock or 2% absolute, whichever is larger, for subspectral areas.
[c]Single measurement on a rock. Measurement uncertainty of 2% absolute for subspectral areas.

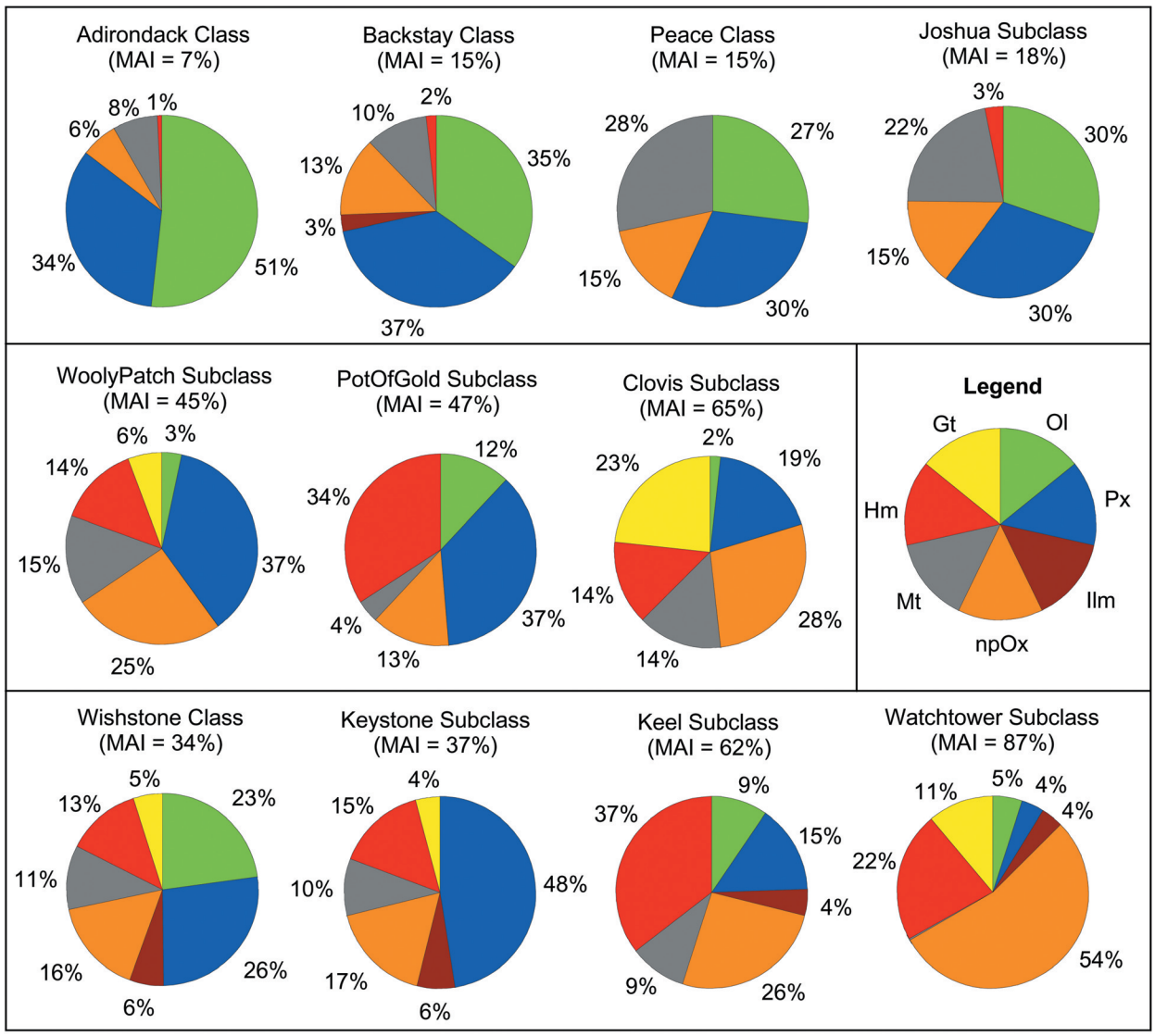

Figure 10. Pie diagrams for the Fe mineralogical composition of rocks according to their classification (Figure 1). Each row is arranged in order of increasing mineralogical alteration (MAI). Relatively unaltered rocks are given in the first row. The second row is highly altered rocks from West Spur, including the Clovis Subclass that has high concentrations of goethite. The third row is the Wishstone and Watchtower rocks that have approximately the same chemical composition but very different mineralogical compositions. All rocks in Wishstone and Watchtower Classes have ilmenite.

under conditions more oxidizing than the magnetite-wustite buffer [e.g., *Nordstrom and Munoz*, 1986] with subsequent weathering to minor npOx + Hm.

4.2.2. Clovis Class (Clovis and WoolyPatch Subclasses) and PotOfGold Subclass

[54] Clovis Class and PotOfGold Subclass rocks are common on West Spur (Figure 9). We divide Clovis Class into Clovis Subclass (Clovis, Ebenezer, Temples, Tetl, Uchben, and Lutefisk) and WoolyPatch Subclass (WoolyPatch) on the basis of mineralogical composition. Clovis Subclass is highly altered (MAI = 65%) has an average of 28% Fe from npOx, 23% from Gt, 19% from Px, 14% each from Mt and Hm, and minor Fe from Ol. The rock Clovis has the highest Fe from Gt of any rock analyzed at Gusev crater as of sol 510. WoolyPatch Subclass rock is much less altered (MAI = 45%) and has an average of ~37% Fe from Px, 25% from npOx, 15% from Mt, 14% from Hm and minor Fe from Gt and Ol. PotOfGold Subclass (PotOfGold, FortKnox, BreadBox, and StringOfPearls) of Other Rocks Class is a group of West Spur rocks that have mineralogical compositions that are different from those for Clovis Class rocks. The subclass has MAI = 47% and has an average of 37% Fe from Px, 34% from Hm, ~12% each from Ol and NpOx, and minor Fe from Mt. In all three subclasses, Fe from pyroxene is substantially greater than Fe from olivine ($A_{Px}/A_{Ol} \sim 3$ and >10 for PotOfGold Subclass and the other two subclasses, respectively). PotOfGold and Keel Subclasses have the highest Fe from Hm of any rock as of Sol 510 ($A_{Hm} = 34-37\%$).

4.2.3. Wishstone Class and Watchtower Class (Watchtower, Keystone, and Keel Subclasses)

[55] All rocks in the Wishstone and Watchtower Classes have a distinctive chemistry with high concentrations of Ti and P and very low concentrations of Cr relative to all other Gusev crater rocks [*Gellert et al.*, 2006; *Ming et al.*, 2006]. Compositional variations among rocks within the two classes are relatively minor [*Ming et al.*, 2006]. The presence of Ilm ($FeTiO_3$) in the MB spectra of all these rocks implies that the high Ti concentrations result from the presence of that mineral. In contrast to the relative compositional homogeneity, the mineralogical composition is highly variable (Table 6). Therefore we divided the Watchtower Class into Keystone (only Keystone analyzed by MB and APXS), Keel (KeelReef and KeelDavis), and Watchtower (Watchtower, Paros, and Pequod) Subclasses, and the subclass values of MAI are 37, 62, and 87% respectively. The MAI of Wishstone Class (Wishstone, WishingWell, Champagne) is lower (34%).

[56] Average Wishstone Class and Keystone Subclass have comparable degrees of alteration and comparable amounts of Fe from Ilm (6%), from npOx (~16%), from Mt (10%), from Hm (14%), and from Gt (4%). The proportions of Fe from Ol and Px are very different. Wishstone Class has approximately equal proportions of Fe from Ol (23%) and Px (26%) and Keystone Subclass has 48% Fe from Px and no detectable Fe from Ol. The rocks in Keel and Watchtower Subclass are highly altered with Fe from Ol + Px less than 24%. Keel Subclass has 37% Fe from Hm, 26% Fe from npOx, 15% from Px, 9% each from Mt and Ol, and 4% from Ilm. Watchtower Subclass, which includes the most oxidized rocks analyzed as of sol 510, has 54% of Fe from npOx, 22% from Hm, 11% from Gt, and 4–5% from each of Ol, Px, and Ilm.

4.3. Possible Impact Origin of Wishstone and Watchtower Class Rocks

[57] The relatively constant chemistry, the diverse mineralogical composition, and the wide range in Fe^{3+}/Fe_T (0.40 to 0.94) in Wishstone and Watchtower Class rocks imply (1) a common progenitor, (2) possible isochemical formation, alteration, and weathering processes, and (3) variable (in time and/or location) environmental conditions during crystallization, alteration, and weathering. Low fluid to rock ratios are implied by isochemical processes. A possible way to meet these constraints is an impact event that involved formation of pools of impact melt and glassy fall-back ejecta. Target materials, if originally heterogeneous, were homogenized with respect to chemical composition during formation of impact melt. Target materials altered in an open hydrologic system prior to the impact event could have atypical basaltic chemical compositions, e.g., corundum normative compositions [*Ming et al.*, 2006]. The impact melt pools and fall-back ejecta are then subject to local conditions during crystallization, alteration, and weathering. These local conditions could range from relatively reducing (e.g., somewhat more oxidizing than the magnetite-wustite buffer) to significantly more oxidizing if the melt pools and fall-back ejecta are invaded by oxidizing fluids and/or vapors. Fe-rich impact melt glass would be highly susceptible to alteration to palagonite-like materials.

[58] In this model, Wishstone Class and Keystone Subclass rocks, now with ~60–70% Fe from Ol + Px + Ilm + Mt, formed in impact melt pools where cooling rates were slow enough to permit crystallization of these minerals. Possibly, the Hm now in these rocks is an alteration product of preexisting magnetite. If so, the original Mt content was ~20–25% Fe from Mt, values which are comparable to Mt contents of the relatively unaltered Peace Class and Joshua Subclass rocks (22–28% Fe in Mt). The explanation for the very different ratios of A_{Ol}/A_{Px} for Wishstone Class (~1) and Keystone Subclass (~0) is not apparent. Possibly, the Wishstone Class rocks (all float rocks) are remnants or impact erratics of original target material, and Keystone Subclass rocks crystallized from impact melt pools. Keel Subclass and especially Watchtower Subclass rocks are heavily altered and now have only 24% and 9%, respectively, Fe from Ol + Px. There may have originally been higher proportions of these phases that were altered during late-stage crystallization and subsolidus cooling when oxidizing fluids and/or vapors invaded the impact melt rocks while they were still hot. The presence of Gt in Watchtower Subclass (11% Fe from Gt) implies at least some aqueous alteration occurred at relatively low temperatures.

[59] Although the target material was not basaltic in composition, the compositional and mineralogical relationships among impact melt rocks at Manicouagan Crater (Quebec, Canada) are akin to the relationships just described for Wishstone and Watchtower rocks. According to *Floran et al.* [1978], there are no statistically significant positional variations in the chemical composition in the Manicouagan impact melt sheet. However, oxidation-state and mineralogical variations [*Floran et al.*, 1976, 1978; *Phinney et al.*, 1978; *Simonds et al.*, 1978; *Morris et al.*,

Table 7. Average Mössbauer Areas for Component Subspectra (f-Factor Corrected) and Fe^{3+}/Fe_T for Classes and Subclasses of Gusev Crater Soils

Generic Name Assignment	Fe2D1 Ol, %	Fe2D2 Px, %	Fe2D3 Ilm, %	Fe3D1 npOx, %	Fe3D2 Sulfate, %	Mt, %	Fe3S1 Mt(tet), %	Fe2.5S1 Mt(oct), %	Fe3S2 Hm, %	Fe3S3 Gt, %	Total, %	Fe^{3+}/Fe_T
Laguna Class												
Average	35	33	0	21	0	9	4	5	2	0	100	0.30
1σ Std. Dev.[a]	5	4	0	6	0	3	2	2	1	0		0.06
Laguna Class, Panda Subclass												
Average	39	35	0	15	0	9	4	5	2	0	100	0.24
1σ Std. Dev.[a]	2	2	0	1	0	2	1	1	2	0		0.02
Laguna Class, Liberty Subclass												
Average	35	34	0	19	0	10	4	6	2	0	100	0.28
1σ Std. Dev.[a]	4	4	0	1	0	2	1	1	1	0		0.02
Laguna Class, Gobi Subclass												
Average	31	32	0	25	0	10	5	5	2	0	100	0.35
1σ Std. Dev.[a]	3	5	0	5	0	5	2	4	1	0		0.06
Laguna Class, Boroughs Subclass												
Average	29	30	0	32	0	9	4	5	2	0	100	0.39
1σ Std. Dev.[a]	3	2	0	3	0	1	1	0	0	0		0.04
PasoRobles Class												
Average	7	9	0	0	65	5	2	4	14	0	100	0.83
1σ Std. Dev.[a]	5	1	0	0	4	1	1	1	9	0		0.05

[a]Standard deviation of class members or 2%, whichever is larger, for subspectral areas.

1995] occur on a scale observed for the Wishstone and Watchtower Class rocks. The oxidation state for Manicouagan rocks ranges from $Fe^{3+}/Fe_T = 0.32$ to 0.92 (~0.4 to 0.94 for Wishstone-Watchtower rocks (Figure 9a) [*Floran et al.*, 1978; *Morris et al.*, 1995]. The Mössbauer mineralogy of the Manicouagan rocks ranges from assemblages dominated by Fe^{2+} from pyroxene and magnetite to assemblages dominated by Fe^{3+} from hematite and phyllosilicates. *Floran et al.* [1978] and *Phinney et al.* [1978] concluded from petrographic observations that smectite formed as a part of the oxidative alteration of glass and mafic minerals (particularly Ol), that relatively large hematite particles formed by oxidative alteration of primary titanomagnetite, and that hematite particles extending in size from micron-sized to submicroscopic particles are formed from glass and mafic minerals. This description might also be appropriate for Wishstone-Watchtower rocks, except that smectite has not been definitively identified by MER instruments. Possible chemical evidence for phyllosilicates is discussed by *Wang et al.* [2006], but there is at present no mineralogical evidence for phyllosilicates [e.g., *Ming et al.*, 2006]. Perhaps the nature of the presumably sulfate-rich oxidizing fluids/vapors on Mars, compared to the Earth, inhibits phyllosilicate formation.

4.4. Mössbauer Mineralogy of Soil and Dust

[60] On the basis of chemical composition, we placed Gusev crater soils into three classes (Figure 1): (1) Laguna Class, (2) PasoRobles Class, and (3) Other Soils Class. Laguna Class soils (all but three soils) have basaltic bulk compositions [*Gellert et al.*, 2006]. The average class and subclass subspectral areas are in Table 7. PasoRobles Class (Pasadena_PasoRobles and PasoRobles2_PasoLight1) have very high concentrations of S compared to Laguna Class soils (~3.2 versus ~0.7 moles/24(O + Cl)). The Other Soils Class includes only the soil Pequod_Doubloon, and its chemical composition is similar to that for Wishstone and Watchtower Class rocks [*Gellert et al.*, 2006; *Ming et al.*, 2006]. Although chemical and mineralogical differences among soils in Laguna Class are not large, we split the class into four subclasses on the basis of MAI index and S concentration: (1) Panda Subclass (MAI = 17%, S = 0.53 moles/24(O + Cl)), (2) Liberty Subclass (MAI = 22%, S = 0.60 moles/24(O + Cl)), (3) Gobi Subclass (MAI = 26%, S = 0.71 moles/24(O + Cl)), and (4) Boroughs Subclass (MAI = 31%, S = 1.1 moles/24(O + Cl)). The boundaries between Panda, Liberty, and Gobi Subclasses are gradational rather than distinct. The Boroughs Subclass includes analyses of subsurface targets in the BigHole and The Boroughs trenches.

[61] Pie diagrams showing the distribution of Fe among Fe-bearing phases are provided in Figure 11. Panda, Liberty, Gobi, and Boroughs Subclasses have, 15–30% Fe from npOx, 31–39% from Ol, 29–35% from Px, 9–10% from Mt, and minor Fe from Hm. Ol decreases and npOx increases from Panda to Liberty to Gobi Subclasses. MAI indices (17–31%) are high compared to Adirondack Class rocks (MAI = 7%), comparable to Backstay Class, Peace Class, Joshua Subclass, and Wishstone Class (MAI = 15–34%, (Figure 10)), and less than Clovis and Watchtower Classes and PotOfGold Subclass (37–87%). Laguna Class soils are mineralogically distinguished from all rocks in the Columbia Hills (as of sol 510) except Backstay Class and Peace Class by their low Hm contents (<3%) and no detectable Gt.

[62] Using various criteria, *Yen et al.* [2005] selected several Gusev surface soils as representative of bright aeolian dust. The one with the best counting statistics is Desert_Gobi, and we take its mineralogical composition as an approximation for Gusev Dust (Figure 11). This view is consistent with the presence of Ol, Px, npOx, and Mt in the MB spectrum of atmospheric dust collected by MER permanent magnets [*Goetz et al.*, 2005]. The counting statistics of the magnet dust spectrum, however, are too

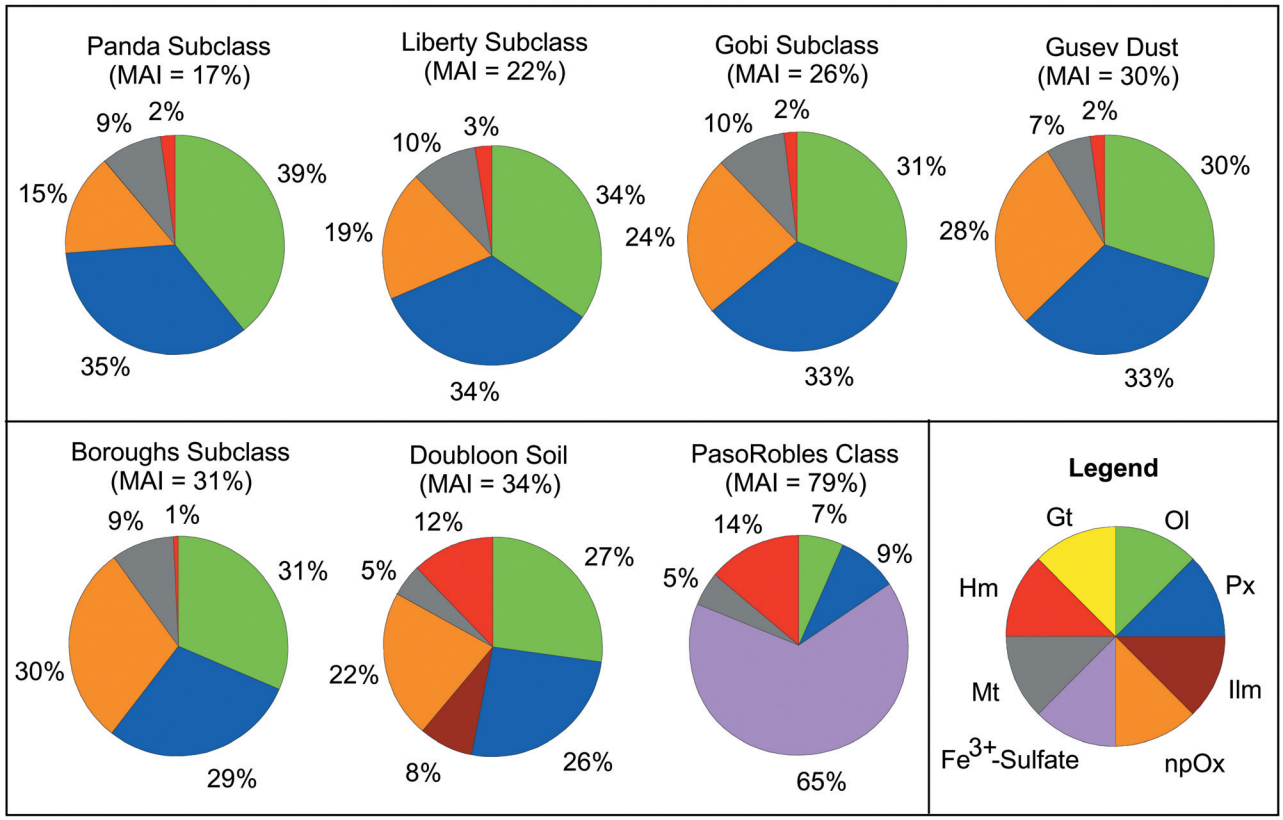

Figure 11. Pie diagrams for the Fe mineralogical composition of soils according to their classification (Figure 1). Each row is arranged in order of increasing MAI. No soil has detectable goethite, and the hematite concentrations in Laguna Class soils and Doubloon soil are comparable to those found in relatively unaltered rocks like Adirondack, Backstay, and Peace Classes and Joshua Subclass. The Fe mineralogical composition of Gusev Dust is similar to that for the soil Desert_Gobi. PasoRobles Class is distinctive because it has high concentrations of Fe^{3+}-sulfate.

poor to permit a detailed comparison to the putative spectrum for Gusev Dust.

[63] PasoRobles Class soils are found as of sol 510 only in one place (downslope from the rock Watchtower on Husband Hill). The class has 65% Fe from Fe^{3+}-sulfate, 14% from Hm, 9% from Px, and 5% from Mt. No other soil has as high a concentration for any single component as PasoRobles Class soil does for Fe^{3+}-sulfate. *Ming et al.* [2006] suggested that PasoRobles is an evaporite deposit that formed via the evaporation of solutions rich in Fe, Mg, Ca, S, P, and Si. The presence of ferric sulfates suggests precipitation from oxidized, low-pH solutions.

4.5. Origin of Soil and Dust

[64] The relative uniformity in chemical composition, Fe oxidation state, and mineralogical composition for Laguna Class soil contrast with the highly variable nature of the corresponding parameters for Gusev crater rocks (Figures 9a, 9b, 10, and 11). In a recent paper examining basaltic soil at both Gusev crater and Meridiani Planum, *Yen et al.* [2005] discuss evidence that high-S, bright dust (i.e., Gusev dust in Figure 11) is a global unit and not dominated by the chemical or mineralogical composition of local rocks. They further argued that low-S, dark soils (i.e., soils in Panda Subclass) could be a global component or be a manifestation of a general similarity of precursor rocks. We next discuss evidence that the former is more likely the case.

[65] As shown in top row of pie diagrams in Figure 11, the trend with increasing MAI is for Fe from Ol to decrease from 39% to 30% and for Fe from npOx to increase from 15% to 28%. The other components vary <2% absolute. These trends suggest that soils may actually be mechanical mixtures of end-members that are more extreme in mineralogical composition than Panda Subclass and Gusev Dust. In Figure 12a, we plot the percentage of Fe from these components as a function of S concentration. We fit the data for each component, and calculated hypothetical rock and dust end-members for S = 0.3 and 1.0 moles/24(O + Cl). The distribution of the Fe-bearing components for the rock (Figure 12b) is similar to that for Adirondack Class for Fe from npOx, Mt, and Hm. Adirondack Class rock is not a suitable precursor Laguna Class soil, however, because the A_{Ol}/A_{Px} ratio for the calculated rock end-member (1.2) is low compared to the ratio for Adirondack Class (1.5) and, more importantly, because Laguna Class soil and Adirondack Class rock have different values of ΔE_Q for Px (2.09–2.12 and 2.06 mm/s, respectively (Table 4)). The calculated dust end-member has $A_{Px} > A_{Ol}$, and a future test of this modeling approach is a MB spectrum of dust on magnets with good counting statistics (see below).

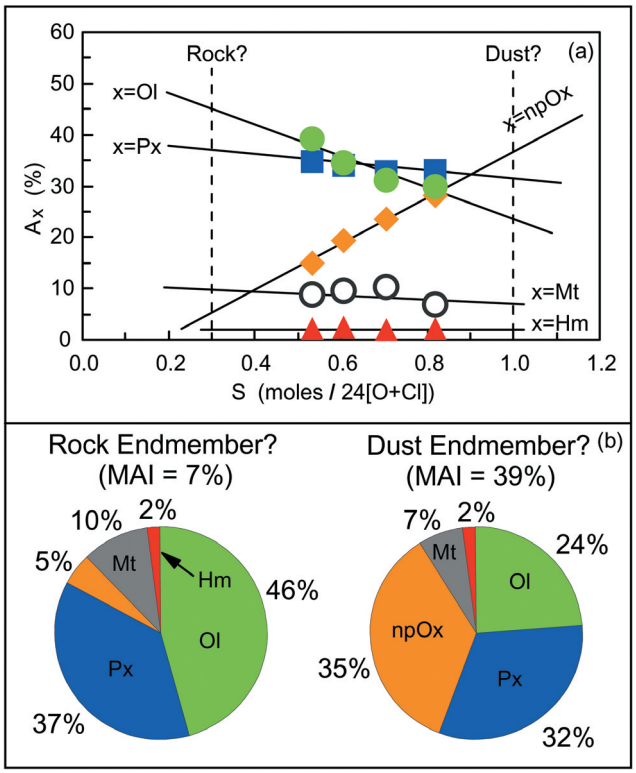

Figure 12. (a) Average relative concentrations of Fe from npOx, Ol, Px, Mt, and Hm in Panda, Liberty, and Gobi Subclasses of soil and Gusev Dust plotted as a function of S concentration. Solid lines are fits to the data, and their intersections with the dashed vertical lines at S = 0.3 and 1.0 moles/24(O + Cl) give the mineralogical composition of hypothetical rock and dust end-members for two-component mixing. (b) Pie diagrams for Fe mineralogical composition hypothetical rock and dust end-members for Laguna Class soils.

[66] The absence of an apparent local rock source for Laguna Class soil in general (i.e., both bright dust and dark soil in the nomenclature of *Yen et al.* [2005]) is evidence that Laguna Class soil is a regional if not a global component. The mineralogical relationship among Laguna Class soil (Figure 12a) could be evolutionary rather than mixing, with only olivine being progressively altered to npOx-bearing phases. Soils and dust are relatively unaltered with abundant Ol, implying that physical weathering, rather than aqueous activity, played the dominant role in forming the basaltic soil and dust present on the Martian surface.

4.6. Magnetic Properties

[67] Permanent magnets on Martian landers and rovers from Viking to Pathfinder to MER have shown that Martian soil and dust have a strongly magnetic component [e.g., *Hargraves et al.*, 1979; *Madsen et al.*, 1999; *Bertelsen et al.*, 2004; *Goetz et al.*, 2005]. For Viking and Pathfinder, the mission teams advocated maghemite as the strongly magnetic component [e.g., *Hargraves et al.*, 1979; *Madsen et al.*, 1999]. Others have argued the component is (titano)-magnetite [e.g., *Coey et al.*, 1990; *Morris et al.*, 1990, 2001]. Recent estimates for the saturation magnetization (J_S) of bulk Martian soil is 1–4 Am^2/kg [*Morris et al.*, 2001; *Madsen et al.*, 2003].

[68] The MER MB results unequivocally show that the double sextet of (titano)magnetite is present in both Martian rock and soil (Figures 2a, 2b, and 2c) and that it is widely dispersed (Figure 13). The MER Magnetic Properties Experiment shows, from analysis of Mössbauer spectra obtained on dust that was attracted to the magnets, that magnetite is also present in the dust [*Goetz et al.*, 2005]. The average concentration of Fe from magnetite ($A_{Mt}Fe_T$/100) in Gusev soil is 0.16 ± 0.08 moles/24(O + Cl). Because Fe in pure magnetite is 18 moles/24(O + Cl) and using, J_S = 92 Am^2/kg [e.g., *Morris et al.*, 1985], the J_s of Gusev soils is 0.8 ± 0.4 Am^2/kg, which is at the low end of the range previously estimated. The most magnetite-rich rock (Peace with $A_{Mt}Fe_T/100 \sim 0.8$) has $J_S \sim 4$ Am^2/kg.

4.7. Mineralogical Evidence for Aqueous Activity

[69] The MER Mössbauer spectrometer, because it is sensitive only to the element Fe, is not directly sensitive to either the H_2O molecule or the hydroxide anion. However, the technique did identify goethite, which has the hydroxide anion as an essential part of its structure (~10% H_2O by weight). Gt-bearing materials were found only in rocks in the Columbia Hills, and the highest concentrations were in rocks at West Spur (Table 6). The rock Clovis has the highest concentration with 40% of Fe from Gt in a target of interior rock exposed by the RAT. This corresponds to ~0.7 wt% H_2O in the rock. Because Gt forms as a product of aqueous activity in natural environments [e.g., *Cornell and Schwertmann*, 1996], the phase is mineralogical evidence for aqueous activity on Mars. NpOx is also likely a H_2O/OH-bearing phase, but we cannot constrain how much is present. The role of water and acid volatiles in the alteration and formation of rocks and outcrops in the Columbia Hill is discussed by *Ming et al.* [2006].

5. Summary

[70] Mössbauer mineralogy was done on more than 82 rock and soil targets by Spirit during its first 510 sols of roving on the plains and Columbia Hills of Gusev crater.

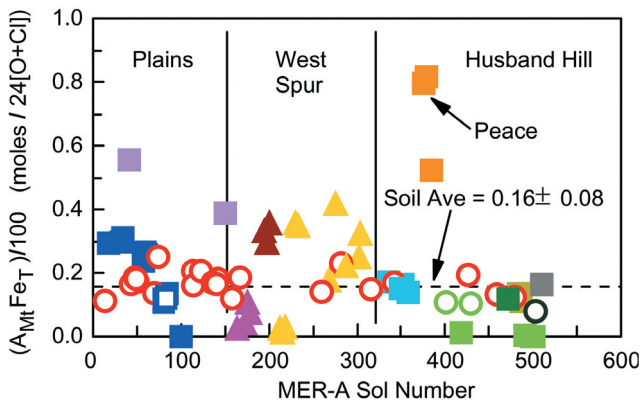

Figure 13. Concentration of Fe from magnetite in rock and soil as a function of location. Magnetite is widely dispersed in rock and soil and accounts for the strongly magnetic properties of soil and dust. Symbols are referenced to the legend in Figure 9.

The elements of Mössbauer mineralogy are the oxidation state of Fe (Fe^{3+}/Fe_T), the identification of Fe-bearing phases, and the distribution of Fe among Fe-bearing phases. The oxidation state can be calculated without mineralogical identification of Fe-bearing phases. Salient results and interpretations as of sol 510 are summarized next.

[71] 1. The oxidation state of Fe for rocks is highly variable, ranging from 0.07 to 0.94 Fe^{3+}/Fe_T. Rocks and soils on the Gusev pains are relatively unaltered. Adirondack Class rock, the most common rock type on the plains, has $Fe^{3+}/Fe_T < 0.20$. Although some rocks in the Columbia Hills are also relatively unaltered (Peace, Wishstone, and Backstay Class rocks), many rocks present as outcrops (Clovis and Watchtower Classes) are pervasively altered (Fe^{3+}/Fe_T = 0.6–0.9).

[72] 2. Eight Fe-bearing phases were identified: Ol, Px, and Ilm as Fe^{2+}-bearing phases, Mt as a Fe^{2+}- and Fe^{3+}-bearing phase, and npOx, Gt, Hm, and a Fe-sulfate as Fe^{3+} bearing phases. The Fe^{3+}-bearing phases, except Mt, are products of oxidative alteration and weathering.

[73] 3. Adirondack, Backstay, and Peace Class rocks and Joshua Subclass rocks are the least altered (MAI = 7–15%). They have <4% Fe from Hm, no detectable Gt, and variable proportions of Fe from Ol, Px, and Mt. These rocks have the highest levels of Fe from Ol + Px (57–85%) and $A_{Ol}/(A_{Ol} + A_{Px}) \sim 0.5$ to 0.6. Adirondack Class and Joshua Subclass rocks are found on the plains, and Backstay and Peace Class rocks are on Husband Hill. Adirondack Class has the largest observed value of Fe from Ol (51%) at Gusev crater.

[74] 4. Wishstone Class and Keystone, WoolyPatch, and PotOfGold Subclasses have moderate levels of alteration (MAI = 34–48%) and have 40–49% Fe from Ol + Px with $A_{Ol}/(A_{Ol} + A_{Px}) \sim 0$ to 0.5. Fe from Hm is large in PotOfGold Subclass (34%) relative to the other groups (13–15%). Wishstone Class and Keystone Subclass rocks are found on Husband Hill, and WoolyPatch and PotOfGold Subclasses are on West Spur. Keystone Subclass has the largest observed Fe from Px (48%) observed at Gusev crater.

[75] 5. Clovis, Keel, and Watchtower Subclasses are pervasively altered (MAI = 62–87%). Clovis and Keel Subclasses have 21–24% Fe from Ol + Px with $A_{Ol}/(A_{Ol} + A_{Px}) \sim 0.1$ to 0.4. Watchtower Subclass has 9% Fe from Ol + Px. Clovis Subclass rocks are confined to West Spur, and Keel and Watchtower Subclass rocks are located on Husband Hill. Clovis, Keel and Watchtower Subclasses have the highest observed values of Fe from Gt (23%), Hm (37%), and npOx (54%), respectively, at Gusev crater.

[76] 6. Ilmenite is detected (<8% Fe from Ilm) in the relatively unaltered Backstay Class rock and in moderately to heavily altered Wishstone and Watchtower Class rocks.

[77] 7. The rock Clovis has 40% Fe from Gt. The presence of Gt is mineralogical evidence for the presence of H_2O/OH on Mars and for aqueous processes.

[78] 8. The relatively constant elemental and very diverse mineralogical composition for Wishstone and Watchtower Class rocks suggests a common progenitor and variable environmental conditions during crystallization, alteration, and weathering. A possible way to do this is an impact event where relatively reducing conditions result in the absence of invasion of the impact melt by oxidizing fluids and/or vapors during late-stage crystallization and subsolidus cooling and relatively oxidizing conditions result where the invasion occurs.

[79] 9. On the basis of elemental and mineralogical composition, Gusev crater soils can be divided into Laguna and PasoRobles Classes. The former, which have ~34% Fe each from Ol and Px, ~19% from npOx, ~10 from Mt, and ~3% from Hm, mineralogically resembles weakly to moderately altered basaltic rocks (average MAI = 22%). Laguna Class includes all except three soils, and the average Fe^{3+}/Fe_T is ~0.3. PasoRobles Class (two soils) has high proportions of Fe present as Fe^{3+} sulfate (~65%). The remaining basaltic soil (Pequod_Doubloon) is not classified with the Laguna Class soils because it contains ilmenite (8% Fe from Ilm).

[80] 10. The strongly magnetic mineral magnetite is ubiquitous in Gusev crater rocks and soils and is the strongly magnetic component in Martian soil and dust.

[81] **Acknowledgments.** R.V.M. and D.W.M. acknowledge support of the NASA Mars Exploration Rover Project and the NASA Johnson Space Center. Development and realization for the MIMOS II Mössbauer spectrometer were funded by the German Space Agency under contract 50QM 99022 and supported by the Technical University of Darmstadt and the University of Mainz. A portion of the work described in this paper was conducted at the Jet Propulsion Laboratory, California Institute of Technology, under a contract with the National Aeronautics and Space Administration. P.A.deS. acknowledges support of CAPES (contract PASJ 142/1999) and CVRD from Brazil. The support of the Russian Space agency is acknowledged. We acknowledge the unwavering support of JPL engineering and MER operations staff and the MER Athena Science Team. We thank M. Madsen and J. Plescia for detailed and thoughtful reviews of the manuscript.

References

Arvidson, R. E., et al. (2004), Localization and physical properties experiments conducted by Spirit at Gusev crater, *Science*, *305*, 821–824.

Arvidson, R. V., et al. (2006), Overview of the Spirit Mars Exploration Rover Mission to Gusev Crater: Landing site to Backstay Rock in the Columbia Hills, *J. Geophys. Res.*, *111*, E02S01, doi:10.1029/2005JE002499.

Bando, Y., M. Kiyama, N. Yamamoto, T. Takada, T. Shinjo, and H. Takaki (1965), Magnetic properties of α-Fe_2O_3 fine particles, *J. Phys. Soc. Jpn.*, *20*, 2086.

Bell, J. F., III, et al. (2004), Pancam multispectral imaging results form the Spirit rover at Gusev crater, *Science*, *305*, 800–806.

Bertelsen, P., et al. (2004), Magnetic properties experiments on the Mars Exploration Rover Spirit at Gusev crater, *Science*, *305*, 827–829.

Bigham, J. M., and D. K. Nordstrom (2000), Iron and aluminum hydroxysulfates from acid sulfate waters, in *Sulfate Minerals: Crystallography, Geochemistry, and Environmental Significance*, *Rev. Mineral. Geochem.*, vol. 40, edited by C. N. Alpers, J. L. Jambor, and D. K. Nordstrom, pp. 351–403, Mineral. Soc. of Am., Washington, D. C.

Bishop, J. L., and E. Murad (1996), Schwertmannite on Mars? Spectroscopic analyses of schwertmannite, its relationship to other ferric minerals, and its possible presence in the surface material on Mars, in *Mineral Spectroscopy: A Tribute to Roger G. Burns*, edited by M. D. Dyar, C. McCammon, and M. W. Schaefer, *Spec. Publ. Geochem. Soc.*, *5*, 337–358.

Burns, R. G., and T. C. Solberg (1990), ^{57}Fe-bearing oxide, silicate, and aluminosilicate minerals: Crystal structure trends in Mossbauer spectra, in *Spectroscopic Characterization of Minerals and Their Surfaces*, *ACS Symp. Ser.*, vol. 415, edited by L. M. Coyne, S. W. S. McKeever, and D. F. Blake, pp. 262–283, Am. Chem. Soc., Washington, D. C.

Christensen, P. R., et al. (2004), Initial results from the Mini-TES experiment in Gusev crater from the Spirit rover, *Science*, *305*, 837–842.

Coey, J. M. D., S. Mørup, M. B. Madsen, and J. M. Knudsen (1990), Titanomaghemite in magnetic soils on Earth and Mars, *J. Geophys. Res.*, *95*, 14,423–14,425.

Cornell, R., and U. Schwertmann (1996), *The Iron Oxides: Structure, Properties, Reactions, Occurrences, and Uses*, 573 pp., John Wiley, Hoboken, N. J.

Dang, M.-Z., D. G. Rancourt, J. E. Dutrizac, G. Lamarche, and R. Provencher (1998), Interplay of surface conditions, particle size, stoichiometry, cell parameters, and magnetism in synthetic hematite-like minerals, *Hyperfine Interact.*, *117*, 271–319.

Daniels, J. M., and A. Rosencwaig (1969), Mössbauer spectroscopy of stoichiometric and non-stoichiometric magnetite, *J. Phys. Chem. Solids*, *30*, 1561–1571.

De Grave, E., and A. Van Alboom (1991), Evaluation of ferrous and ferric Mössbauer fractions, *Phys. Chem. Miner.*, *18*, 337–342.

De Grave, E., and R. E. Vandenberghe (1990), Mössbauer effect study of the spin structure in natural hematites, *Phys. Chem. Miner.*, *17*, 344–352.

de Souza, P. A., Jr. (1999), Automation in Mössbauer spectroscopy analysis, *Lab. Robot. Autom.*, *11*, 13–23.

Dyar, M. D., and M. W. Schaefer (2004), Mossbauer spectroscopy on the surface of Mars: Constraints and expectations, *Earth Planet. Sci. Lett.*, *218*, 243–259.

Floran, R. J., C. H. Simonds, R. A. Grieve, W. C. Phinney, J. L. Warner, M. J. Rhodes, B. M. Jahn, and M. R. Dence (1976), Petrology, structure and origin of the Manicouagan melt sheet, Quebec, Canada: A preliminary report, *Geophys. Res. Lett.*, *3*, 49–52.

Floran, R. J., R. A. Grieve, W. C. Phinney, J. L. Warner, C. H. Simonds, D. P. Blanchard, and M. R. Dence (1978), Manicougan impact melt, Quebec: 1. Stratigraphy, petrology, and chemistry, *J. Geophys. Res.*, *83*, 2737–2759.

Gellert, R., et al. (2006), Alpha Particle X-Ray Spectrometer (APXS): Results from Gusev Crater and calibration report, *J. Geophys. Res.*, *111*, E02S05, doi:10.1029/2005JE002555.

Goetz, W., et al. (2005), Indication of drier periods on Mars from the chemistry and mineralogy of atmospheric dust, *Nature*, *436*(7), doi:10.1038/nature03807.

Gütlich, P., R. F. Link, and A. Trautwein (1978), *Mössbauer Spectroscopy and Transition Metal Chemistry*, Springer, New York.

Hargraves, R. B., D. W. Collinson, R. E. Arvidson, and P. M. Cates (1979), Viking magnetic properties experiment: Extended mission results, *J. Geophys. Res.*, *84*, 8379–8384.

Haskin, L. A., et al. (2005), Water alteration of rocks and soils from the Spirit rover site, Gusev crater, Mars, *Nature*, *436*, 66–69.

Klingelhöfer, G., et al. (2003), Athena MIMOS II Mössbauer spectrometer investigation, *J. Geophys. Res.*, *108*(E12), 8067, doi:10.1029/2003JE002138.

Lane, M. D., M. D. Dyar, and J. L. Bishop (2004), Spectroscopic evidence for hydrous iron sulfate in the Martian soil, *Geophys. Res. Lett.*, *31*, L19702, doi:10.1029/2004GL021231.

Madsen, M. B., S. F. Hviid, H. P. Gunnlaugsson, W. Goetz, C. T. Pedersen, A. R. Dinesen, C. T. Mogensen, M. Olsen, R. B. Hargraves, and J. M. Knudsen (1999), The magnetic properties experiments on Mars Pathfinder, *J. Geophys. Res.*, *104*, 8761–8779.

Madsen, M. B., et al. (2003), Magnetic Properties Experiments on the Mars Exploration Rover mission, *J. Geophys. Res.*, *108*(E12), 8069, doi:10.1029/2002JE002029.

McCammon, C. (1995), Mössbauer spectroscopy of minerals, in *A Handbook of Physical Constants: Mineral Physics and Crystallography*, *AGU Ref. Shelf Ser.*, vol. 2, edited by T. J. Ahrens, pp. 332–347, AGU, Washington, D. C.

McSween, H. Y., et al. (2004), Basaltic rocks analyzed by the Spirit Rover in Gusev crater, *Science*, *305*, 842–845.

McSween, H. Y., et al. (2006), Characterization and petrologic interpretation of olivine-rich basalts at Gusev Crater, Mars, *J. Geophys. Res.*, *111*, E02S10, doi:10.1029/2005JE002477.

Ming, D. W., et al. (2006), Geochemical and mineralogical indicators for aqueous processes in the Columbia Hills of Gusev crater, Mars, *J. Geophys. Res.*, *111*, E02S12, doi:10.1029/2005JE002560.

Morris, R. V., H. V. Lauer Jr., C. A. Lawson, E. K. Gibson Jr., G. A. Nace, and C. Stewart (1985), Spectral and other physicochemical properties of submicron powders of hematite (α-Fe_2O_3), maghemite (γ-Fe_2O_3), magnetite (Fe_3O_4), goethite (α-FeOOH), and lepidocrocite (γ-FeOOH), *J. Geophys. Res.*, *90*, 3126–3144.

Morris, R. V., D. G. Agresti, H. V. Lauer Jr., J. A. Newcomb, T. D. Shelfer, and A. V. Murali (1989), Evidence for pigmentary hematite on Mars based on optical, magnetic, and Mössbauer studies of superparamagnetic (nanocrystalline) hematite, *J. Geophys. Res.*, *94*, 2760–2778.

Morris, R. V., J. J. Gooding, H. V. Lauer Jr., and R. B. Singer (1990), Origins of Marslike spectral and magnetic properties of a Hawaiian palagonitic soil, *J. Geophys. Res.*, *95*, 14,427–14,434.

Morris, R. V., D. C. Golden, J. F. Bell III, H. V. Lauer Jr., and J. B. Adams (1993), Pigmenting agents in Martian soils: Inferences from spectral, Mössbauer, and magnetic properties of nanophase and other iron oxides in Hawaiian palagonitic soil PN-9, *Geochim. Cosmochim. Acta*, *57*, 4597–4609.

Morris, R. V., D. C. Golden, J. F. Bell III, and H. V. Lauer Jr. (1995), Hematite, pyroxene, and phyllosilicates on Mars: Implications from oxidized impact melt rocks from Manicouagan Crater, Quebec, Canada, *J. Geophys. Res.*, *100*, 5319–5328.

Morris, R. V., et al. (2000), Mineralogy, composition, and alteration of Mars Pathfinder rocks and soils: Evidence from multispectral, elemental, and magnetic data on terrestrial analogue, SNC meteorite, and Pathfinder samples, *J. Geophys. Res.*, *105*, 1757–1817.

Morris, R. V., D. C. Golden, D. W. Ming, T. D. Shelfer, L. C. Jørgensen, J. F. Bell III, T. G. Graff, and S. A. Mertzman (2001), Phyllosilicate-poor palagonitic dust form Mauna Kea Volcano (Hawaii): A mineralogical analogue for magnetic Martian dust?, *J. Geophys. Res.*, *106*, 5057–5083.

Morris, R. V., et al. (2004), Moessbauer mineralogy on Mars: First results from the Spirit landing site in Gusev Crater, *Science*, *305*, 833–836.

Murad, E., and J. H. Johnston (1987), Iron oxides and oxyhydroxides, in *Mössbauer Spectroscopy Applied to Inorganic Chemistry*, Vol. 2, edited by G. J. Long, pp. 507–582, Springer, New York.

Myneni, S. C. B. (2000), X-ray and vibrational spectroscopy of sulfate in Earth materials, in *Sulfate Minerals: Crystallography, Geochemistry, and Environmental Significance*, *Rev. Mineral. Geochem.*, vol. 40, edited by C. N. Alpers, J. L. Jambor, and D. K. Nordstrom, pp. 113–172, Mineral. Soc. of Am., Washington, D. C.

Nordstrom, D. K., and J. L. Munoz (1986), Mineral equilibria III. Oxidation-reduction reactions, in *Geochemical Thermodynamics*, pp. 285–324, Blackwell Sci., Malden, Mass.

Phinney, W. C., C. H. Simonds, A. Cochran, and P. E. McGee (1978), West Clearwater, Quebec impact structure, Part II: Petrology, *Proc. Lunar Planet. Sci. Conf. 9th*, 2659–2693.

Ramdani, A., J. Steinmetz, C. Gleitzer, J. M. D. Coey, and J. M. Friedt (1987), Pertubation de l'exchange electronique rapide par les lacunes cationiques dans $Fe_{3-x}O_4$($x \leq 0.09$), *J. Phys. Chem. Solids*, *48*, 217–228.

Rancourt, D. G. (1996), Analytical methods for Mössbauer spectral analysis of complex materials, in *Mossbauer Spectroscopy Applied to Magnetism and Materials Science*, vol. 2, edited by G. J. Long and F. Grandjean, pp. 105–124, Springer, New York.

Rieder, R., et. al. (2004), Chemistry of rocks and soils at Meridiani Planum from the Alpha Particle X-ray Spectrometer, *Science, 306*, 1746–1749.

Rossman, G. R. (1980), Pyroxene spectroscopy, in *Pyroxenes*, *Rev. Mineral.*, vol. 7, edited by C. T. Prewitt, pp. 93–115, Mineral. Soc. of Am., Washington, D. C.

Simonds, C. H., R. J. Floran, P. E. McGee, W. C. Phinney, and J. L. Warner (1978), Petrogenesis of melt rocks, Manicouagan impact structure, Quebec, *J. Geophys. Res.*, *83*, 2773–2788.

Squyres, S. W., et al. (2003), Athena Mars rover science investigation, *J. Geophys. Res.*, *108*(E12), 8062, doi:10.1029/2003JE002121.

Squyres, S. W., et al. (2004), The Spirit Rover's Athena science investigation at Gusev crater, Mars, *Science*, *305*, 794–799.

Squyres, S. W., et al. (2006), Rocks of the Columbia Hills, *J. Geophys. Res.*, *111*, E02S11, doi:10.1029/2005JE002562.

Stevens, J. G., A. M. Khasanov, J. W. Miller, H. Pollak, and Z. Li (Eds.) (1998), *Mössbauer Mineral Handbook*, 527 pp., Biltmore Press, Ashville, N. C.

Tanaka, H., and M. Kono (1987), Mössbauer spectra on titanomagnetite: A reappraisal, *J. Geomagn. Geoelectr.*, *39*, 463–475.

Wang, A., et al. (2006), Evidence of phyllosilicates in Wooly Patch, an altered rock encountered at West Spur, Columbia Hills, by the Spirit rover in Gusev Crater, Mars, *J. Geophys. Res.*, *111*, E02S16, doi:10.1029/2005JE002516.

Yen, A. S., et al. (2005), An integrated view of the chemistry and mineralogy of Martian soils, *Nature*, *436*(7), doi:10.1038/nature03637.

R. E. Arvidson, Department of Earth and Planetary Sciences, Washington University, Campus Box 1169, One Brookings Drive, St. Louis, MO 63130, USA.

B. Bernhardt, P. A. de Souza Jr., I. Fleischer, J. Foh, P. Gütlich, G. Klingelhöfer, F. Renz, D. S. Rodionov, and C. Schröder, Institut für Anorganische und Analytische Chemie, Johannes Gutenberg-Universität, D-55128 Mainz, Germany.

U. Bonnes and E. Kankeleit, Darmstadt University of Technology, D-64289 Darmstadt, Germany.

E. N. Evlanov and B. Zubkov, Space Research Institute IKI, 117997 Moscow, Russia.

R. Gellert, Department of Physics, University of Guelph, Guelph, ON, Canada N1G 2W1.

D. W. Ming and R. V. Morris, NASA Johnson Space Center, Mail Code SN3, Houston, TX 77058, USA. (richard.v.morris@nasa.gov)

S. W. Squyres, Center for Radiophysics and Space Research, Cornell University, Ithaca, NY 14853, USA.

T. Wdowiak, Department of Physics, University of Alabama at Birmingham, Birmingham, AL 35294, USA.

A. Yen, Jet Propulsion Laboratory, California Institute of Technology, Pasadena, CA 91109, USA.